High coverage whole genome sequencing of the expanded 1000 Genomes Project cohort including 602 trios.

Marta Byrska-Bishop*[,1,@], Uday S. Evani*[,1], Xuefang Zhao*[,2,3,4], Anna O. Basile[1], Haley J. Abel[5,6], Allison A. Regier[5,6], André Corvelo[1], Wayne E. Clarke[1], Rajeeva Musunuri[1] , Kshithija Nagulapalli[1], Susan Fairley[7], Alexi Runnels[1], Lara Winterkorn[1], Ernesto Lowy-Gallego[7], The Human Genome Structural Variation Consortium[8], Paul Flicek[7], Soren Germer[1], Harrison Brand[2,3,4,9], Ira M. Hall[5,6,10,11], Michael E. Talkowski[2,3,4,9], Giuseppe Narzisi[1], Michael C. Zody[1,@].

*** These authors contributed equally to this work.**

[@] Correspondence should be addressed to: mczody@nygenome.org (M.C.Z.) and mbyrska-bishop@nygenome.org (M.B.).

1. New York Genome Center, New York, NY, USA.
2. Program in Medical and Population Genetics, Broad Institute of MIT and Harvard, Cambridge, MA, USA.
3. Center for Genomic Medicine, Massachusetts General Hospital, Boston, MA, USA.
4. Department of Neurology, Massachusetts General Hospital and Harvard Medical School, Boston, MA, USA.
5. McDonnell Genome Institute, Washington University School of Medicine, St. Louis, MO, USA.
6. Department of Medicine, Washington University School of Medicine, St. Louis, MO, USA.
7. European Molecular Biology Laboratory, European Bioinformatics Institute, Wellcome Genome Campus, Hinxton, Cambridge, CB10 1SD, UK.
8. List of the HGSVC authors and corresponding affiliations are at the end of the manuscript.
9. Stanley Center for Psychiatric Research, Broad Institute of MIT and Harvard, Cambridge, MA, USA.
10. Center for Genomic Health, Yale University School of Medicine, New Haven, CT, USA.
11. Department of Genetics, Yale University School of Medicine, New Haven, CT, USA.

ABSTRACT

The 1000 Genomes Project (1kGP), launched in 2008, is the largest fully open resource of whole genome sequencing (WGS) data consented for public distribution of raw sequence data without access or use restrictions. The final (phase 3) 2015 release of 1kGP included 2,504 unrelated samples from 26 populations, representing five continental regions of the world and was based on a combination of technologies including low coverage WGS (mean depth 7.4X), high coverage whole exome sequencing (mean depth 65.7X), and microarray genotyping. Here, we present a new, *high coverage* WGS resource encompassing the original 2,504 1kGP samples, as well as an additional 698 related samples that result in 602 complete trios in the 1kGP cohort. We sequenced this expanded 1kGP cohort of 3,202 samples to a targeted depth of 30X using Illumina NovaSeq 6000 instruments. We performed SNV/INDEL calling against the GRCh38 reference using GATK's HaplotypeCaller, and generated a comprehensive set of SVs by integrating multiple analytic methods through a sophisticated machine learning model, upgrading the 1kGP dataset to current state-of-the-art standards. Using this strategy, we defined over 111 million SNVs, 14 million INDELs, and ~170 thousand SVs across the entire cohort of 3,202 samples with estimated false discovery rate (FDR) of 0.3%, 1.0%, and 1.8%, respectively. By comparison to the low-coverage phase 3 callset, we observed substantial improvements in variant discovery and estimated FDR that were facilitated by high coverage re-sequencing and expansion of the cohort. Specifically, we called 7% more SNVs, 59% more INDELs, and 170% more SVs per genome than the phase 3 callset. Moreover, we leveraged the presence of families in the cohort to achieve superior haplotype phasing accuracy and we demonstrate improvements that the high coverage panel brings especially for INDEL imputation. We make all the data generated as part of this project publicly available and we envision this updated version of the 1kGP callset to become the new de facto public resource for the worldwide scientific community working on genomics and genetics.

INTRODUCTION

The 1000 Genomes Project (1kGP) was the first large scale whole genome sequencing (WGS) effort to deliver a catalog of human genetic variation[1–4]. The project sampled participants from 26 populations across 5 continental regions of the world. Spanning seven years of data generation and analysis, it culminated in 2015 with a publication of the final, phase 3, variant callset[3,4] consisting of 2,504 unrelated samples, a subset of which is from the HapMap collection[5]. The set of 2,504 samples was selected with the goal to maximize the discovery of single nucleotide variants (SNVs) at minor allele frequencies (MAF) of 1% or higher in diverse populations, hence related samples were not included. The phase 3 callset was generated based on the combination of low coverage WGS (mean depth 7.4X), high-coverage whole exome sequencing (WES, mean depth 65.7X), and microarray genotyping data. It included 84.7 million SNVs, and 3.6 million short insertions and deletions (INDELs), as well as a separate set of 60,000 structural variants (SVs; alterations ≥50bp). The 1kGP resources have been collectively cited over 15,000 times to date and have been utilized for foundational applications such as genotype imputation, eQTL mapping, variant pathogenicity prioritization, population history, and evolutionary genetics studies[6–15]. While the phase 3 dataset captured the vast majority of common variants (MAF > 1%) in the population (>99% of SNVs and >85 % INDELs)[3], detection of rare variants (MAF <= 1%) was limited due to low sequencing coverage outside of the coding regions of the genome.

Here, we present high coverage WGS and comprehensive analyses of the original 2,504 1kGP samples, as well as additional 698 related samples. These related samples were not included as part of the phase 3 callset, but now provide complete WGS on 602 trios in the 1kGP cohort. A small subset of these pedigrees have been sequenced previously as part of various efforts, such as Platinum Genomes[16], Complete Genomics[3], and the Human Genome Structural Variant Consortium (HGSVC), which generated long-read WGS from Pacific Biosciences (PacBio), Bionano Genomics, and Strand-seq technology[17,18]; however, this is the first time that nearly all 1kGP trios have been sequenced at high coverage and jointly analyzed for the discovery and genotyping of genomic variation across the size and frequency spectrum, ranging from SNVs to large and complex SVs in a singular resource. We sequenced the expanded cohort of 3,202 samples to a targeted depth of 30X (minimum 27X, mean 34X) genome coverage using Illumina NovaSeq 6000 instruments. We aligned reads to the GRCh38 reference and performed SNV/INDEL calling using GATK's HaplotypeCaller. Using this strategy, we called over 111 million SNVs and over 14 million INDELs with false discovery rate (FDR) of 0.3% and 1.0%, respectively, across the entire cohort of 3,202 samples. We also discovered and genotyped a comprehensive set of SVs, including insertions, deletions, duplications, inversions, and multiallelic copy number variants (CNVs), by integrating multiple algorithms and analytic pipelines[19,20]. Comparison with previous low coverage sequencing performed in phase 3 of the 1kGP demonstrated significant improvements in sensitivity and specificity in the SNV, INDEL and SV callsets, highlighting that the re-sequencing effort and expansion of the cohort to include trios brought significant value to the field.

One of the major applications of the phase 3 1kGP callset has been its widespread use as a reference panel for variant imputation in sparse, array-based genotyping data with a goal of improving the statistical power of downstream genome-wide association studies (GWAS) and facilitating fine-mapping of causal variants. We leveraged the presence of full trios in the expanded 1kGP cohort and performed haplotype phasing of SNVs and INDELs using a

statistical phasing approach with pedigree-based correction. We demonstrate the power that inclusion of family members has on improving the accuracy of phasing and show how it compares to the phase 3 version. Finally, we evaluate the imputation performance of the high coverage panel and demonstrate improvements especially in INDEL imputation as compared to the phase 3 panel.

Over the past few years, the cost of high coverage WGS has decreased dramatically which, combined with substantial progress in analytics tools, has contributed to the emergence of several population-scale high coverage WGS panels, such as the Genome Aggregation Database (gnomAD; 15,708 WGS and 125,848 WES samples)[21], Trans-Omics for Precision Medicine (TOPMed: https://www.nhlbiwgs.org/; 138,000 samples)[22], or the UK Biobank (UKBB: https://www.ukbiobank.ac.uk/; goal to sequence 500,000 samples by 2023) to name a few. These growing resources, many fold larger in sample size than the 1kGP cohort, enable continuous expansion of the catalog of genetic variation in the human population and facilitate discoveries that improve human health. Unlike the 1kGP, most of the recent large scale WGS efforts have restrictions on public data sharing as they are often linked to clinical data, which amplifies privacy concerns. As a consequence, only aggregate population-level allele frequencies are available for public access in most cases. In contrast, samples within the 1kGP cohort have been consented for full public release of genetic information which allows for unrestricted sharing of the complete sample-level genotype (GT) data. This enables granting access to a downloadable reference imputation panel, as well as use of the dataset for methods development and benchmarking, among other applications. All the data generated as part of this project including BAM files, VCFs, and functional annotations, has been made publicly available (see the Data Access section). We envision this updated version of the 1kGP cohort to become the new de facto public resource for the worldwide scientific community working on genomics and genetics.

RESULTS

Overview of SNV and INDEL calls across the 3,202 1kGP samples. We performed WGS of the original 2,504 1kGP unrelated samples as well as additional 698 related samples, which completed 602 parent-child trios in the 1kGP cohort and brought the total number of sequenced samples to 3,202 (Figure 1A, Table S1). The final variant callset across the 3,202 samples contains 111,048,944 SNVs and 14,435,076 INDELs. The mean SNV density across the callable genome was 39.46 per 1kb of sequence. Chromosome X (30.16 SNVs per 1kb) displayed the lowest density across all chromosomes, followed by chromosome 1 (36.46 SNVs per 1kb) among the autosomes, whereas chromosome 19 (43.21 SNVs per 1kb) had the highest density overall (Table S2). Figure 1B summarizes variant counts by alternate allele frequency (AF), restricted to unrelated samples to prevent overestimation of AF in the population. We found 74,264,978 (59.2%) variants were singletons (allele count (AC) = 1) or doubletons (AC = 2); 33,008,491 (26.3%) variants to be rare (AC > 2 and AF <= 0.01), and 18,210,551 (14.5%) variants to be common (AF > 0.01). Overall, we found 19,239,888 (15.3%) total variants called were novel, defined as not reported in dbSNP build 151. Among the novel variants, 83.5% are singletons or doubletons, 11.8% are rare, and 4.6% are common variants. As expected, we see a higher percentage of novel variants among singleton and doubleton categories.

The callset contains 117,175,809 variant sites of which 6.5% (7,676,044) are multiallelic. We divided the genome into easy, medium, and hard regions as defined in the CCDG functional equivalence paper[23]. Easy refers to parts of the genome that are mostly unique and where we can confidently call variants, hard is made up of low complexity and repetitive regions, and any region that did not fall into the two categories was classified as medium. We looked at the distribution of multiallelic sites across the three sets of regions and found that although hard regions only make up 8% of the genome they contain 38% of all the multiallelic sites, compared to easy regions that make up 70% and contain 40% of sites. About 50% of the sites in hard regions are multiallelic but that drops down to ~15% in the filtered phased callset (described in the "Haplotype phasing of high quality SNVs and INDELs" section) suggesting that many of these variants might be of poor quality. This is not surprising as hard regions are made up of low complexity and repeat elements that make it harder to call variants confidently.

At a per sample level, we called an average of 5,038,683 small variants total (Figure 1C, top panel). This includes an average of 4,080,991 SNVs, 420,645 short insertions, and 451,276 short deletions per genome, across samples from all populations (Figure 1C, bottom 3 panels; mixed and complex variants and multi-nucleotide polymorphisms (MNPs) were not included in the breakdown). We observed an average transition to transversion ratio (Ti/Tv) of 2.01 and heterozygous to non-reference homozygous ratio (Het/Hom) of 1.70 (Figure S1), consistent with expectations for WGS data. As expected, the average number of variant sites was higher in the individuals from African populations, with 4,653,521 SNVs, 465,797 short insertions, and 503,995 short deletions per genome. In line with that, we also observed a higher Het/Hom ratio of 2.03 among the AFR samples (Figure S1). We also noticed higher variability in the number of variants in individuals belonging to the admixed American population. On average, we called 21,800 novel variant sites per sample across all populations, with African and South Asian populations containing more novel sites than Europeans, East Asians, and Admixed Americans (Figure S2).

Lastly, we determined the FDR of the high coverage callset by comparing genotype calls from sample NA12878 to the high confidence calls from the Genome in a Bottle (GIAB) NA12878 callset[24] (see precision vs. recall plot in Figure S3). Using this approach, we calculated an FDR of 0.3% for SNVs with sensitivity of 99.7%, and an FDR of 1% for INDELs with sensitivity of 98%.

Overview of structural variation across the 3,202 1kGP samples. We generated an SV callset across all 3,202 1kGP samples with short read sequencing data. These SV genotypes were discovered and integrated from three analytic pipelines: GATK-SV[19], svtools[20] and Absinthe (see Methods, Table S5). This final ensemble callset included 170,242 loci, comprised of 89,269 deletions, 24,068 duplications, 674 multiallelic CNVs (mCNVs), 51,829 insertions, 956 inversions, 3,430 complex SVs (CPX) consisting of a combination of multiple SV signatures, and 16 inter-chromosomal translocations (CTX, Figure 2A). The size and allele frequency distribution of SVs followed expectations; Mobile element signatures were observed for ALU (200-300 bp), SVA (1-2 kb), and LINE1 (5-6 kb) variants. Most SVs were rare, and SV allele frequencies were inversely correlated with SV size (Figure 2B, C). On average, ~9,266 SVs were discovered in each genome (see Figure 2D). The distribution of SVs observed per individual followed expectations for ancestry with the greatest number of SVs per genome derived from African populations (Figure 2E)[25]. The specificity of the SV callset was also quite

high, with a *de novo* SV rate of 1.8%, which represents the combination of false positive SVs in children, false negative SVs in parents, and cell line artifacts in probands (Figure 2F).

Comparison of SNV and INDEL calls against the 1kGP phase 3 callset. We compared our SNV and INDEL calls against the phase 3 callset to quantify the improvements brought by high coverage sequencing and pipeline upgrades. A direct comparison to the original callset was not possible as the phase 3 dataset was aligned to the GRCh37 reference. To overcome this issue, we used the GRCh38 version of the phase 3 callset, which was generated by dbSNP, European Genome-phenome Archive (EGA), and European Variation Archive (EVA)[26] by lifting over the coordinates of variant sites using dbSNP build 149[27]. Due to the high number of liftover failures on chromosomes X and Y, the comparison was limited to autosomes. On average, about 10,465 sites failed to liftover in autosomes, whereas the number of sites that failed to liftover in chromosome X and Y was 2,020,268 and 55,528, respectively. The liftover failures occur when the coordinate position has been moved to a different chromosome in the new build or due to inability to resolve the reference allele or strand changes. For consistency, we limited the comparison of the SNV/INDEL calls to the 2,504 samples that are common between the high coverage and the phase 3 datasets.

When restricted to autosomes, the 2,504-sample high coverage callset included 94.84 million SNVs and 9.08 million INDELs, as compared to 78.24 million SNVs and 3.15 million INDELs in the phase 3 callset. Figure 3A,B shows the breakdown of SNVs and INDELs from the two datasets into singleton (AC=1), rare (AC > 1 and AF <= 0.01), and common (AF > 0.01) bins based on non-reference AF. We called ~15 million more singleton SNVs and ~4 million more rare SNVs in high coverage as compared to phase 3, whereas the number of common variants remained similar. We called ~3 times more INDELs in the high coverage callset, with increase in INDEL counts observed across the entire AF spectrum. The phase 3 callset contained only 4,377 singleton INDEL calls, as compared to 2,999,027 in the high coverage dataset. The low number of ultra-rare INDEL calls in the phase 3 set can be attributed to more stringent filtering applied to INDELs as compared to biallelic SNVs, as INDELs were harder to call with low coverage sequencing[3]. We also called significantly more longer INDELs. The lifted-over phase 3 set contains only 17 INDELs that are >50bp in size, whereas the high coverage callset contains 192,583 calls in this size range (Figure S4). Notably, the original phase 3 callset on GRCh37 contained 2,285 INDELs that are >50bp with the largest being 661bp insertion. We suspect the larger INDELs failed liftover and did not make it into the GRCh38 callset.

Overall, we recalled 94.7% of phase 3 variants in the high coverage callset. More than 95% of phase 3 variants in the easy genomic regions were recalled in the high coverage callset, compared to 88% and 73% in medium and hard regions, respectively (Figure 3C). The SNV recall rate was higher than the INDEL recall rate in the easy and medium regions whereas it was lower in the hard regions, suggesting there might be more false positives among SNV calls in the hard regions. We observed high correlation of AF among shared variants between the high coverage and phase 3 callsets, with Spearman correlation coefficient (rho) of >0.95 for both SNV and INDEL across all regions, except for INDELs in the hard region where it drops to 0.9 (Figure 3D).

At a per sample level, there are ~4.3 million variant sites on average in the phase 3 dataset compared to ~4.9 million in the high coverage set (Figure 3E). On average, 84% of variant loci called per sample in the high coverage callset were discovered in phase 3. We calculated FDR

of the 2,504-sample high coverage and the phase 3 callsets by comparing the genotype calls from sample NA12878 to high confidence calls for the same sample from the GIAB[24]. We excluded any variants from both the callsets that fell into regions in GRCh38 that could not be lifted over from GRCh37 (see Table S3). Overall the FDR among SNVs was 0.3% in the high coverage, compared to 1.2% in the phase 3 callset. Among INDELs, FDR was 1.1% in the high coverage as compared to 12.6% in the phase 3 callset. Figure 3F shows FDR for the two sets in rare (AF <= 0.01), common (AF > 0.01 and AF <= 0.05), and very common (AF > 0.05) AF bins. As expected, in both callsets, FDR for SNVs decreases for high AF variants. We see the opposite trend for phase 3 INDELs because there are very few calls in the rare and common AF bins compared to very common.

Evaluation of the SV callset against the 1kGP phase 3 callset. This ensemble SV callset was benchmarked against the 1kGP phase 3 SVs (7.4X average coverage)[4] on the 2,504 shared samples to assess the quality and unique value brought by high coverage sequencing and genotyping capabilities of new analytic pipelines. The current ensemble SV callset discovered over two-fold more SV sites than phase 3 (166,752 vs. 68,698), and encompassed 87.4% of the phase 3 SV calls (Figure 4A). This increased sensitivity and high overlap of phase 3 SVs was consistent across all SV classes (Figure 4A), and per genome, with an average of 9,266 SVs detected in the current ensemble callset compared to 3,431 SVs in the phase 3 callset (Figure 4B).

The high coverage SV callset provided significant added value in terms of the discovery of SVs that alter gene function by comparison to the phase 3 low-coverage SV dataset. Consistent with previous large population studies[19], we observed that biallelic SVs in each genome resulted in probable loss of function (pLoF) of 119 protein coding genes, complete copy gain (CG) of 24 genes, and duplications of intragenic exons (IED) of 6 genes. The same analyses of the low-coverage phase 3 callset predicted an average of 32 genes disrupted by SVs per genome (30 pLoF, 1 CG and 1 IEDs; Figure 4C). The 1kGP dataset also offered an estimate in the population diversity of functional SV variation, where African populations had the highest number of pLoF SVs per genome, (Figure 4D), with similar patterns observed for CG and IED SVs that altered protein coding gene sequences (Figure S11).

Haplotype phasing of high quality SNVs and INDELs. We performed haplotype phasing of high quality autosomal SNVs and INDELs across the 3,202-sample 1kGP cohort using statistical phasing with pedigree-based correction, as implemented in the SHAPEIT2-duohmm software[28,29]. Phasing of the high quality SNVs and INDELs on chromosome X was performed using statistical phasing, as implemented in the Eagle2 software[30], which, unlike SHAPEIT2-duohmm, supports ploidy-aware phasing. We defined high quality SNVs and INDELs by applying the following set of filtering criteria: 1) VQSR PASS; 2) GT missingness rate < 5%; 2) Hardy Weinberg Equilibrium (HWE) exact test[31] p-value > 1e-10 in at least one of the 5 super-populations (EUR, EAS, SAS, AMR, AFR); and 3) mendelian error rate (MER) for sites with complete trio calls ≤ 5%. Additionally, we excluded all sites with minor allele count (MAC) < 2, as singletons are not informative for phasing. The resulting set of high quality variants that went into phasing consisted of 72,065,314 sites on chromosome 1-22 and chromosome X (Figure 5A), which included 61,411,215 SNVs, 9,954,481 INDELs, and 699,618 MNPs (counts at the ALT allele-level) (Figure S5).

We evaluated phasing accuracy of the phased panel by computing switch error rate (SER) among pairs of consecutive heterozygous sites in sample NA12878 (child in a full trio in the expanded 3,202-sample cohort). As the phasing truth set against which the evaluation was performed, we used the extensively validated, haplotype-resolved Platinum Genome NA12878 callset generated by Illumina[16]. The SER among SNVs and INDELs across all autosomes was 0.074% (1,754 switches among 2,338,955 assessed SNV/INDEL heterozygous pairs), indicating high accuracy of phasing. As expected, chromosome X, which was phased without pedigree-based correction, displayed higher SER as compared to autosomes (SER=0.491%; 362 switches among 73,794 assessed SNV/INDEL heterozygous pairs total; Figure S6; Table S4). We did not observe a significant difference in phasing accuracy between SNVs and INDELs, other than on chromosome X, where SER for INDELs was 2.01% (187 switches among 9,298 assessed INDEL heterozygous pairs total) as compared to 0.51% for SNVs (328 switches among 64,583 assessed SNV heterozygous pairs total) (Figure S7). In addition to assessing SER genome-wide, we also assessed it at the following four MAF bins: 1) (0%, 0.1%]; 2) (0.1%, 1%]; 3) (1%, 10%]; and 4) (10%, 50%]. While we noticed an expected increase in SER with decrease in MAF, the SER remained low throughout the entire MAF spectrum, reaching a maximum of 1.2% in the (0, 0.1%] MAF bin across autosomes (Figure 5B, violet solid line; see Figure S6 for per chromosome breakdown). Such high phasing accuracy at the low end of the MAF spectrum can be attributed to both the presence of family members in the expanded 1kGP cohort (Figure 5B, dashed violet line with open triangles vs. dashed violet line with open diamonds) as well as to pedigree-based correction applied after statistical phasing (Figure 5B, solid violet line vs. dashed violet line with open triangles).

Finally, we compared phasing accuracy of the high coverage family-based panel against the phase 3 panel. The phase 3 panel was phased using statistical phasing with family-based scaffold (built from chip array data on the entire 1kGP cohort including related samples), without pedigree-based correction, as no trios were sequenced as part of the phase 3 panel[3]. We observed an order of magnitude lower SER in the high coverage as compared to the phase 3 panel, across the entire MAF spectrum (Figure 5B, solid violet vs. solid aqua line). This significant improvement in SER underscores the power that inclusion of trios has on the quality of haplotype phasing in the upgraded panel. It is worth noting that the phasing accuracy of the 2,504-sample phase 3 dataset was slightly better than that of the 2,504-sample high coverage dataset (Figure 5B, solid aqua line vs. dashed violet line with open diamonds) due to the fact that the latter dataset was phased using statistical phasing alone, without the family-based scaffold.

Imputation performance of the high coverage 3,202-sample SNV/INDEL panel. To assess imputation performance, we imputed a set of 279 diverse samples from the Simons Genome Diversity Project (SGDP)[32] using IMPUTE2 software[33] with the high coverage and the phase 3 panels separately as the reference. We evaluated the accuracy of imputed genotypes by computing the squared correlation (R^2) between imputed allele dosages and dosages from WGS data across 110 samples, 22 from each of the five super-populations (the maximum number of samples in all populations). For the high coverage panel, the aggregate R^2 between imputed SNV genotypes and WGS genotypes for EUR and SAS samples reaches 0.88 at an AF of 0.2%, and increases at more common variant frequencies (Figure 5C). Imputation of AFR, EAS, and AMR samples attains an $R^2 \geq 0.8$ at AF of 3%, 5%, and 5%, respectively. In general, INDELs are imputed with lower accuracy than SNVs, reaching an $R^2 > 0.8$ at an alternate allele frequency of 5% in EUR and SAS samples, and 20% in AFR, EAS, and AMR samples. Figures

5D and 5E compare the imputation accuracy of the phase 3 and high coverage panels for SNVs and INDELs across sites shared between the panels. Using the high coverage reference panel leads to a significant increase in imputation performance compared to the phase 3 panel for SNVs and INDELs across all super-populations. These differences are largest for EUR (high coverage panel SNP R^2=0.98 at 0.1% AF; phase 3 panel SNP R^2=0.49 at 0.1% AF) and SAS samples (high coverage panel SNP R^2=0.99 at 0.2% AF; phase 3 panel SNP R^2=0.85 at 0.2% AF). Differences in imputation performance between the panels are most pronounced for INDELs which see a 9.6-fold increase in the accuracy of imputing EUR samples (AF=0.1%), 4.2-fold increase in SAS (AF=0.2%), 8.9-fold increase in AFR (AF=0.1%), 0.29-fold increase in EAS (AF=0.1%), and 9-fold increase in AMR (AF=0.2%) samples when using the high coverage panel.

DISCUSSION

We present results from *high coverage* WGS of the expanded 1kGP cohort, consisting of 2,504 original samples as well as additional 698 related samples, completing 602 trios in the cohort. We called >111 million SNVs, >14 million INDELs, and ~170,000 SVs across the 3,202 samples, using state-of-the-art methods. When compared to the low coverage phase 3 1kGP dataset published in 2015, the variant counts in the high coverage callset reflect an estimated increase of 258,505 SNVs (1.07-fold), 321,965 INDELs (1.59-fold), and 5,835 (2.7-fold) SVs per genome, and a cohort-level increase of 16.6 million SNV, 5.9 million INDEL, and ~100 thousand SV loci, across the original 2,504 unrelated samples. As expected, given that the phase 3 dataset identified nearly all common SNVs (MAF > 1%) in the population, the vast majority of the new SNVs identified here were in the rare MAF spectrum (AC ≤ 2). Since limitations of the low coverage sequencing had a greater negative impact on INDEL as compared to SNV calling in the phase 3 dataset, we observed gains in INDEL counts across the entire MAF spectrum, with gains in the rare end of the spectrum being the most pronounced.

We acknowledge that a *direct* comparison of the high coverage 1kGP SNV/INDEL dataset against the phase 3 set was impossible due to differences in genomic builds that were used for variant calling during generation of the two callsets. To address this, we used a version of the phase 3 dataset that was lifted over from the GRCh37 to the GRCh38 reference. As a result, over 2 million variants (99% of which are on chromosomes X and Y) that failed the lift-over had to be excluded from the comparative analysis. Importantly, we were not positioned to dissect the impact of various factors that likely contributed to differences in variant calls between the high coverage and phase 3 datasets. Differences in sequencing platforms and read length (phase 3: Illumina HiSeq 2000 and HiSeq 2500, 76 bp or 101 bp paired-end reads; high coverage: Illumina NovaSeq 6000, 150 bp paired-end reads), library preparation (phase 3: PCR-based; high coverage: PCR-free), sequencing coverage (phase 3: mean depth 7.4X; high coverage: mean depth 34X), reference genome (phase 3: GRCh37; high coverage: GRCh38), alignment software (phase 3: BWA 0.5.9; high coverage: BWA-MEM 0.7.15), as well as in downstream bioinformatics pipeline most likely all contributed to various degrees to the differences in variant calls that we described here. Overall, despite major differences in data generation and analysis, we found high concordance between the high coverage and the phase 3 SNV/INDEL callset. Nearly 95% of small variants from the phase 3 callset were recalled in the high coverage

dataset with AF correlation of 0.90-0.975, depending on the region of the genome.

The SVs presented here provide a significant increase over the phase 3 callset, both in the number of SVs detected per genome (9,266 vs. 3,431) and in the number of SVs predicted to directly alter gene function (149 vs. 32 per genome) across these populations. Notably, one limitation of the 1kGP dataset is the use of cell line DNA, which can include somatic mutations that arise during cell proliferation. In agreement with the Polaris project[34], we observed aneuploidy of allosomes in 0.94% of the samples, and sub-chromosomal level mosaic CNVs on multiple autosomes (Figure S12). We further performed manual inspection of all large CNVs (>50Kb, n = 3717), as well as benchmarked large inversions against Strand-seq (n = 256), and the variants that lack support were labeled as 'LowQual' in the SV callset so that they can be easily excluded from future analyses. This data, coupled with the availability of inheritance information from 602 complete trios and the independent availability of long read WGS, Strand-seq, and optical mapping data on 34 of these samples[18], provides an unprecedented open access SV resource for methods development and genomic studies.

Inclusion of 602 trios in the expanded 1kGP cohort led to high accuracy of SNV/INDEL haplotype phasing due to both an increase in long-range haplotype sharing between related samples which facilitates phasing, and pedigree-based correction applied after statistical phasing to ensure consistency of phased haplotypes with the pedigree structure. We also demonstrate that the phased high coverage SNV/INDEL panel exhibits an order of magnitude higher phasing accuracy as compared to the phase 3 dataset across the entire MAF spectrum. Importantly, improvements in small variant calling, coupled with higher phasing accuracy of the high coverage panel, translated into significantly better imputation accuracy, especially for INDELs, across all of the 1kGP super-populations when the high coverage panel was used as the reference for imputation as compared to the phase 3 panel.

For more than a decade, the 1000 Genomes collection has been a key resource in the field of genomics. These datasets have produced scientific insights into population genetics and genome biology, as well as provided an openly sharable resource that has been widely used in methods development and testing as well as for technical validation. By generating high coverage sequencing data for the complete phase 3 set of 2,504 unrelated individuals and completing 602 trios with 698 additional samples, we have updated this critical resource with benchmarks and standards for a new generation of large-scale international whole genome sequencing initiatives. Our state of the art SNV, INDEL, and SV callsets, freely released, provide the most accurate and comprehensive catalog of variation compiled to date across this diverse genomic resource, particularly in rare SNVs and all classes of indels and SVs that were challenging to detect using earlier sequencing and analysis methods on low coverage data. We also present an improved phasing and imputation panel leveraging full sequence from trios that outperforms the existing imputation panels. Importantly, this panel is fully public and can be freely downloaded and used in combination with other panels and for use with any target dataset. Although many larger sequencing projects have now been conducted, the open nature of the 1000 Genomes samples will continue to make this a foundational resource for the community in the years to come.

METHODS

Data collection, WGS library preparation and sequencing. DNA extracted from lymphoblastoid cell lines (LCL) was ordered from the Coriell Institute for Medical Research for each of the 3,202 1kGP samples. Whole genome sequencing (WGS) libraries were prepared using the Truseq DNA PCR-free (450bp) Library Preparation Kit in accordance with the manufacturer's instructions. Briefly, 1ug of DNA was sheared using a Covaris LE220 sonicator (adaptive focused acoustics). DNA fragments underwent bead-based size selection and were subsequently end-repaired, adenylated, and ligated to Illumina sequencing adapters. Final libraries were evaluated using fluorescent-based assays including qPCR with the Universal KAPA Library Quantification Kit and Fragment Analyzer (Advanced Analytics) or BioAnalyzer (Agilent 2100). Libraries were sequenced on an Illumina Novaseq 6000 sequencer using 2 x 150bp cycles.

Alignment and SNV/INDEL calling. Read alignment to the human reference genome GRCh38, duplicate marking, and Base Quality Score Recalibration (BQSR) were performed according to the functional equivalence pipeline standard developed for the Centers for Common Disease Genomics project [23]. SNV and INDEL calling was performed using GATK version 3.5, as described below. For variant discovery we used HaplotypeCaller in GVCF mode[35] with sex-dependent ploidy settings on chromosome X and Y. Specifically, variant discovery on chromosome X was performed using diploid settings in females, diploid settings on PAR regions in males, and haploid settings on non-PAR regions in males. Variant discovery on chromosome Y was performed with haploid settings in males and was skipped entirely in females. We combined GVCFs in batches of ~200 samples using CombineGVCFs and joint-genotyped all 3,202 samples with GenotypeGVCFs. We then used VariantRecalibrator to train the Variant Quality Score Recalibration (VQSR) model using "maxGaussians 8" and "maxGaussians 4" parameters for SNVs and INDELs, respectively. We applied the VQSR model to the joint callset using ApplyRecalibration with truth sensitivity levels of 99.8% for SNVs and 99.0% for INDELs. Variant annotations were performed using SnpEff [36] and BCFtools[37]. SnpEff was used to annotate variant effect prediction and BCFtools was used to annotate membership and allele frequency from various variant databases like 1kGP phase 3[3], cosmic (v79) (https://cancer.sanger.ac.uk/cosmic)[38], dbNSFP (v3.2a)[39,40], dbSNP (v151)[27] and ExAC (v0.3)[41].

Quality control of sequence data. We ran a number of quality control (QC) tools to look for quality issues, sample swaps, and contamination issues. We ran FastQC (https://www.bioinformatics.babraham.ac.uk/projects/fastqc/) on the raw sequence data to assess yield and raw base qualities. We ran Picard CollectMultipleMetrics and CollectWGSMetrics (http://broadinstitute.github.io/picard/) on the aligned BAM to collect alignment and insert size metrics. Picard CollectGcBiasMetrics was run to compute normalized coverage across multiple GC bins. Reads duplication metrics were quantified by running Picard MarkDuplicates on the BAM.

All the samples had at least 27X mean coverage across the genome (average per sample coverage: 34X, range: 27X-71X) and at least 91% of the bases at base quality score 30 or higher (Figure S8A, B). The mean duplicate rate across the samples was 9% but there were 5 samples that had a duplicate rate greater than 20 (Figure S8C). The median per sample insert size was 433 bp (Figure S8D). Higher duplication rate is a known issue with Illumina's patterned flow cell that uses exclusion amplification clustering method to increase data output, but this

chemistry is very sensitive to library loading concentrations. Higher loading concentrations can lead to low throughput because of polyclonal clusters being formed in the nanowells of the patterned flow cell, whereas low concentration can lead to pad hopping which increases the duplication rate. VerifyBamID[42] was run in chip-free mode to estimate the likelihood of sample contamination. We use a cutoff of 2% to flag any sample for contamination and none of the samples reached the cutoff.

To make sure there were no sample mix-ups we ran genotype concordance against genotyping chip data. For that, we used the chip data that was released with phase 3. We did not find chip data for 15 samples in phase 3 so for those we ran Infinium CoreExome-24 v1.3 chip and performed genotype concordance. All the samples had >97% genotype concordance.

BCFTools was used to split multiallelic variants into multiple rows and normalize INDELs before performing cumulative variant counts. Per sample variant metrics were collected using GATK VariantEval. The reference genome sequence was divided into three categories: Easy, Medium, and Hard, as defined in the functional equivalence of genome sequencing analysis pipelines paper[23]. The Easy genomic regions consist of GIAB gold standard high confidence regions. These are regions with mostly unique sequences where variant calling can be performed confidently. The Hard regions consist of centromeres, microsatellite repeats, low complexity regions, and windows determined to have high copy number. Any sequence that did not fall into either Easy or Hard regions was classified as Medium. FDR was calculated by comparing variant calls on sample NA12878 from the 3,202 callset to the high confidence variant calls from the GIAB version 3.3.2 on the same sample. The VCF files were compared using hap.py (v0.3.12; github.com/Illumina/hap.py) using the rtg-tools (v3.8.2)[43] vcfeval comparison engine. For FDR calculation the variant comparison was restricted to the confident regions as defined by the GIAB.

Comparison of the high coverage SNV/INDEL calls against the phase 3 dataset. To compare the high coverage against the phase 3 callset, we used the GRCh38 lifted over version of the phase 3 callset, as described in https://www.internationalgenome.org/announcements/updated-GRCh38-liftover/. Due to the high number of liftover failures on chromosomes X and Y we restricted the comparison to autosomes. Additionally, for FDR comparative analysis against the phase 3 callset, we excluded regions in GRCh38 that could not be lifted over from GRCh37 prior to computing FDR. This was done by going over each interval in GRCh38 GIAB confident regions and trying liftover to GRCh37 using CrossMap[44]. Any interval or part of the interval that either failed to liftover or lifted over to a different chromosome were part of the exclusion criteria. Overall only 0.1% of bases were excluded from the GIAB confident regions due to liftover issues. When we applied the exclusion list to the 2,504 high coverage callset, 7,486 variants were filtered out and 526 were filtered out from the phase 3 callset. See Table S3 for the percentage of bases in GRCh38 that were part of the exclusion list broken down by chromosome.

SV discovery using GATK-SV. GATK-SV involved an ensemble SV discovery and refinement pipeline for WGS data. The technical details of the method were previously described in Collins et al[19] for application to the genome aggregation database (gnomAD) for SV discovery, and further described in analyses from the HGSVC[18]. In this study, the same methods were applied to all 3,202 samples for SV discovery. In brief, SVs discovered by Manta, Wham, MELT, cn.MOPS and GATK-gCNV from Ebert et al. were integrated, genotyped across all samples,

resolved for complex SVs, and annotated for variant class and functional impact. The FDR was previously assessed from analyses in quartet families, which yielded a 97% molecular validation rate for *de novo* SV predictions[45], as well as a 94% validation rate compared to long-read sequencing[19].

SV discovery using svtools. The svtools[46] method was previously described in Abel et al[20] and applied for SV discovery across 17,795 genomes from the Centers for Common Disease Genomics (CCDG) program.[20] The workflow combines per-sample variant discovery with lumpy[47] and manta[48] with resolution-aware cross-sample merging. The set of merged variants is then genotyped with svtyper[49], followed by copy-number annotation with cnvnator[50] and reclassification of variants based on concordance of read-depth with breakpoint orientation. All parameter settings and versions are as implemented in the wdl-based work (https://github.com/hall-lab/sv-pipeline).

Large insertion discovery using Absinthe. On a per-sample basis, insertions with a minimum length of 100bp were discovered through *de novo* assembly of unmapped and discordant read pairs using Absinthe (github.com/nygenome/absinthe), and then genotyped using Paragraph[51], respecting sex-specific ploidies. Insertion calls from all 3,202 samples that were positively genotyped with a PASS filter flag were then clustered by genomic location and aligned using MAFFT[52]. For each locus, the most consensual allele was selected. Variants from the resulting merged callset were then re-genotyped on all 3,202 individuals. To produce the final callset only variants with 1) genotyping PASS filter rate >= 80%; 2) Mendelian Error Rate <= 5% for complete trio calls; and 3) HWE Chi-square test p-value > $1e^{-6}$ in at least one of the 5 super-populations were kept.

Integration of GATK-SV, svtools, and Absinthe callsets. We conducted a series of analyses to benchmark SVs from each of the three methods described above, including their false discovery rate (FDR) as indicated by inheritance rates and support from orthogonal technologies, as well as their breakpoint precision estimated by the deviation of their SV breakpoints from long read assemblies in three genomes from analyses in the HGSVC[17]. We also compared the three callsets to decide on the optimal integration strategy to maximize sensitivity and minimize FDR in the final ensemble callset (Table S6). Details of the comparison and integration strategies are described separately for insertions and all other variant classes below.

Integration of insertions from GATK-SV and Absinthe. We compared the *de novo* rate of variant calls from each pipeline for insertions, yielding results of 4.1% for GATK-SV, 25.8% for svtools, and 2.4% for Absinthe. Given these results we restricted integration of insertions to GATK-SV and Absinthe. Each insertion pair was considered concordant if the insertion points were within 100 bp. The FDR of each insertion callset was estimated from three measurements: 1. *de novo* rate of SVs observed in the 602 trios; 2. proportion of SVs that were not validated by VaPoR[53], an algorithm that evaluates SV quality by directly comparing raw PacBio reads against the reference genome, and 3. proportion of SVs that were not overlapped by SVs from PacBio assemblies in the same genome (Figure S9D). Precision of an insertion call was estimated by the distance of the insertion point to the closest PacBio insertion and the difference between the length of inserted sequence versus the length of the closest PacBio insertion calculated as an odds ratio. Both insertion callsets display less than 5% FDR based on inheritance and PacBio support, and the callsets were thus merged for all subsequent analyses (Figure S9D). Notably,

as Absinthe showed higher precision than GATK-SV, as measured from both the coordinates of the insertion point and the length of inserted sequences (Figure S9H, I), we retained the Absinthe record for insertions that were shared by both methods.

Integration of deletions, duplications, and inversions from GATK-SV and svtools. To consider a pair of SVs of the same variant class other than insertions as concordant, 50% reciprocal overlap was required for SVs larger than 5 kb and 10% reciprocal overlap was required for variants under 5 kb respectively. The FDR across variant calls was evaluated using the same measurements as described above. For deletions, duplications, and inversions, we observed low FDR (<5%) among variants that were shared by GATK-SV and svtools, but significantly higher FDR in the subset that were uniquely discovered by either algorithm (Supp Figure S9E-G). To restrict the final callset to high-quality variants, a machine learning model (lightGBM[54]) was trained on each SV class. Three samples that were previously analyzed in the HGSVC studies (HG00514, HG00733, NA19240)[17,18] were selected to train the model. The truth data was defined by SVs that were uni-parentally inherited, shared by GATK-SV and svtools, supported by VaPoR, and overlapped by PacBio callsets. The false training subset was selected as SVs that appeared as *de novo* in offspring genomes, specifically discovered by either GATK-SV or svtools, not supported by VaPoR, and not overlapped by PacBio callsets. Multiple features were included in the model, including the sequencing depth of each SV, the depth of the 1kb region around each SV, the count of aberrant pair ends (PE) within 150 bp of each SV, the count of split reads (SR) within 100 bp of each breakpoints, the size, allele fraction and genomic location (split into short repeats, segmental duplications, all remaining repeat masked regions, and the remaining unique sequences) of each SV, and the fraction of offspring harbor a *de novo* variant among trios in which the SV is observed. Each SV per genome was assigned a 'boost score' by the lightGBM model, and SVs with >0.448 boost score were labeled as 'PASS' in the model (Figure S9M, N). This threshold was specifically selected to retain an estimated FDR < 5%. Callset specific SVs that failed the lightGBM model in less than 48% of all examined samples were included in the final integrated callst (Figure S9N).

To design strategies to merge SVs shared by GATK-SV and svtools, the precision of SV calls was evaluated by examining the distance between breakpoint coordinates of SVs to matched calls in the PacBio callset. Comparable breakpoint precision was observed for GATK-SV and svtools (Figure S9J-L). Thus, for SVs in each sample, the variant with the greatest number of split reads for each breakpoint was selected, or if equivalent then the variant with the higher boost score was retained, then for each locus the SV observed in the greatest number of samples was retained as final.

Inclusion of mCNV, CPX and CTX variants from GATK-SV. Other minority SVs types, including mCNVs, CPX and CTX, were specifically detected by GATK-SV, so we performed in-depth manual inspection to ensure their quality before including them in the final integration callset. The depth profile across all 3,202 samples around each mCNV was plotted for manual review, and mCNVs that did not show clear stratification among samples were labeled as 'Manual_LQ' in the filter column even if they showed clear deviation from the normal copy number of 2 (Figure S10). For CTX, the aberrantly aligned read-pairs across each breakpoint was manually examined, and variants that lacked sufficient support were labeled as 'Manual_LQ' in the final callset.

Haplotype phasing. For haplotype phasing we used statistical phasing with pedigree-based correction, as implemented in the SHAPEIT2-duohmm software[28,29]. Phasing with SHAPEIT2-duohmm was performed per chromosome using the default settings, except for the window size "-W" which was increased from 2Mb (default) to 5Mb to account for increased amounts of shared IBD due to pedigrees being present in the dataset (as recommended in the SHAPEIT2 manual). SHAPEIT2 does not handle multiallelic variant phasing. To phase both biallelic and multiallelic variants, we first split the multiallelic sites into separate rows, while left-aligning and normalizing INDELs, using the *bcftools norm* tool [37]. We then shifted the position of multiallelic variants (2nd, 3rd, etc ALT alleles) by 1 or more bp (depending on how many ALT alleles there are at a given position) to ensure a unique start position for all variants, which is required for SHAPEIT2. The positions were shifted back to the original ones after phasing. SHAPEIT2 duohmm supports phasing of autosomal variants only. Therefore, to phase variants on chromosome X we used statistical phasing as implemented in the Eagle2 software[30]. Phasing with Eagle2 was performed using default parameters. No shifting of positions for multiallelic sites was needed as Eagle2 supports phasing of variants with the same start site. Phasing accuracy evaluation was performed using the WhatsHap *compare* tool[55]. As a measure of phasing accuracy we used switch error rate (SER), which is defined as:

$$\text{SER} = \frac{\textit{number of switch errors}}{\textit{number of assessed HET pairs}}$$

In all of the evaluations, SER was computed for sample NA12878 relative to the Platinum Genome NA12878 gold standard truth set [16].

Imputation performance evaluation. We performed imputation on 279 samples from 130 diverse populations using WGS data from the Simons Genome Diversity Project (SGDP) [32]. To create a pseudo-GWAS dataset, we extracted the genotypes at all sites included on an Illumina Infinium Omni2.5-8 v1.4 array. We performed quality control (QC) of the dataset using standard pre-imputation filters, removing sites which did not meet at least one of the following criteria: genotype call rate of >= 95%, MAF > 1%, and HWE p-value >= $1e^{-4}$. We used plink software [56] for all QC steps, and analysis was restricted to the autosomes. We imputed the data passing quality control with the phase 3 and the high coverage panels, separately. For the phase 3 reference panel, we used the low coverage 1000 Genomes phased SNV set called directly against GRCh38 by EBI. SHAPEIT2[28] was used to perform a strand check of the dataset and remove any problematic sites as determined by aligning with the respective panel. We pre-phased the data using SHAPEIT2 and an input reference panel. We imputed the pre-phased data using the IMPUTE2[33] software with default parameters. Following imputation, we concatenated the imputed intervals to create an autosome-wide imputed dataset with each of the panels. We evaluated imputation using 22 samples from each of the five super-populations (EUR, AFR, SAS, EAS, and AMR) and compared the held out imputed genotypes with the WGS genotypes stratified by MAF. For this evaluation, we converted the posterior genotype probabilities produced by IMPUTE2 to dosages using QCTOOL version 2.0.2 (www.well.ox.ac.uk/~gav/qctool_v2/), and the WGS genotypes to dosages using BCFtools[37]. For the data imputed with the high coverage panel, we computed the squared correlation (R^2) between the imputed dosages and those from the WGS data for all non-missing sites. To compare imputation accuracy between the phase 3 and the high coverage panels, we restricted the evaluations to only sites shared between the two panels.

DATA ACCESS

To download the bam files, SNV/INDEL VCF, SV VCF, as well as the filtered haplotype-resolved SNV/INDEL callset, please visit:
https://www.internationalgenome.org/data-portal/data-collection/30x-grch38.
Sequence data was deposited in ENA under projects PRJEB31736 and PRJEB36890.

ACKNOWLEDGEMENTS

The following cell lines/DNA samples were obtained from the NIGMS Human Genetic Cell Repository at the Coriell Institute for Medical Research: [NA06984, NA06985, NA06986, NA06989, NA06991, NA06993, NA06994, NA06995, NA06997, NA07000, NA07014, NA07019, NA07022, NA07029, NA07031, NA07034, NA07037, NA07045, NA07048, NA07051, NA07055, NA07056, NA07340, NA07345, NA07346, NA07347, NA07348, NA07349, NA07357, NA07435, NA10830, NA10831, NA10835, NA10836, NA10837, NA10838, NA10839, NA10840, NA10842, NA10843, NA10845, NA10846, NA10847, NA10850, NA10851, NA10852, NA10853, NA10854, NA10855, NA10856, NA10857, NA10859, NA10860, NA10861, NA10863, NA10864, NA10865, NA11829, NA11830, NA11831, NA11832, NA11839, NA11840, NA11843, NA11881, NA11882, NA11891, NA11892, NA11893, NA11894, NA11917, NA11918, NA11919, NA11920, NA11930, NA11931, NA11932, NA11933, NA11992, NA11993, NA11994, NA11995, NA12003, NA12004, NA12005, NA12006, NA12043, NA12044, NA12045, NA12046, NA12056, NA12057, NA12058, NA12144, NA12145, NA12146, NA12154, NA12155, NA12156, NA12234, NA12239, NA12248, NA12249, NA12264, NA12272, NA12273, NA12274, NA12275, NA12282, NA12283, NA12286, NA12287, NA12329, NA12335, NA12336, NA12340, NA12341, NA12342, NA12343, NA12344, NA12347, NA12348, NA12375, NA12376, NA12383, NA12386, NA12399, NA12400, NA12413, NA12414, NA12485, NA12489, NA12546, NA12707, NA12708, NA12716, NA12717, NA12718, NA12739, NA12740, NA12748, NA12749, NA12750, NA12751, NA12752, NA12753, NA12760, NA12761, NA12762, NA12763, NA12766, NA12767, NA12775, NA12776, NA12777, NA12778, NA12801, NA12802, NA12812, NA12813, NA12814, NA12815, NA12817, NA12818, NA12827, NA12828, NA12829, NA12830, NA12832, NA12842, NA12843, NA12864, NA12865, NA12872, NA12873, NA12874, NA12875, NA12877, NA12878, NA12889, NA12890, NA12891, NA12892].

These data were generated at the New York Genome Center with funds provided by NHGRI Grants 3UM1HG008901-03S1 and 3UM1HG008901-04S1. A.C., W.E.C., and M.C.Z. were partially supported by NHGRI grant UM1HG008901. S.F., E.L., and P.F. were partially supported by the Wellcome Trust (WT104947/Z/14/Z) and the European Molecular Biology Laboratory. Support for analyses by X.Z. and M.E.T. was provided by NIMH MH115957-02. **Competing interests**: M.C.Z. is a shareholder in Merck & Co and Thermo Fisher Scientific. P.F. is a member of the scientific advisory boards of Fabric Genomics, Inc., and Eagle Genomics, Ltd. J.L. is an employee and shareholder of Bionano Genomics.

AUTHOR CONTRIBUTIONS

Writing of the manuscript and figure generation: M.B., U.S.E., X.Z., A.O.B.
SNV/INDEL calling: U.S.E., M.B.
SNV/INDEL analysis: U.S.E., M.B., A.O.B., R.M.

SV calling: X.Z., H.B., H.A., A.A.R., A.C., W.E.C., The Human Genome Structural Variant Consortium.
SV integration and analysis: X.Z., H.B.
Production and quality control of the WGS data: L.W., A.R., U.S.E., M.B., K.N.
Data coordination, data sharing, and user support: S.F., E.L., P.F.
These authors jointly supervised this work: S.G., I.M.H., M.E.T, G.N., M.C.Z.

CONSORTIA

The Human Genome Structural Variation Consortium: Evan E. Eichler[1,2], Jan O. Korbel[3], Charles Lee[4,5], Scott E. Devine[6], William T. Harvey[1], Weichen Zhou[7], Ryan E. Mills[7], Tobias Rausch[3], Sushant Kumar[8], Can Alkan[9,10], Fereydoun Hormozdiari[11], Zechen Chong[12], Xiaofei Yang[4,13,14], Jiadong Lin[15], Mark B. Gerstein[8], Ye Kai[15], Qihui Zhu[4], Feyza Yilmaz[4].

1. Department of Genome Sciences, University of Washington School of Medicine, 3720 15th Ave NE, Seattle, WA 98195-5065, USA.
2. Howard Hughes Medical Institute, University of Washington, Seattle, WA 98195, USA.
3. European Molecular Biology Laboratory (EMBL), Genome Biology Unit, Meyerhofstr. 1, 69117 Heidelberg, Germany.
4. The Jackson Laboratory for Genomic Medicine, 10 Discovery Dr, Farmington, CT 06030, USA.
5. Precision Medicine Center, The First Affiliated Hospital of Xi'an Jiaotong University, 277 West Yanta Rd., Xi'an, 710061, Shaanxi, China.
6. Institute for Genome Sciences, University of Maryland School of Medicine, 670 W Baltimore Street, Baltimore, MD 21201, USA.
7. Department of Computational Medicine & Bioinformatics, University of Michigan, 500 S. State Street, Ann Arbor, MI 48109, USA.
8. Program in Computational Biology and Bioinformatics, Yale University, BASS 432&437, 266 Whitney Avenue, New Haven, CT 06520, USA.
9. Department of Computer Engineering, Bilkent University, Ankara, 06800, Turkey.
10. Bilkent-Hacettepe Health Sciences and Technologies Program, Bilkent University, Ankara, 06800, Turkey.
11. Department of Biochemistry and Molecular Medicine, MIND Institute and Genome Center, University of California, Davis, CA 95616, USA.
12. Department of Genetics and Informatics Institute, School of Medicine, University of Alabama at Birmingham, Birmingham, AL 35294, USA.
13. Department of Computer Science and Technology, School of Electronic and Information Engineering, Xi'an Jiaotong University, Xi'an, 710049, China.
14. MOE Key Lab for Intelligent Networks & Networks Security, School of Electronics and Information Engineering, Xi'an Jiaotong University, Xi'an, 710049, China.
15. School of Automation Science and Engineering, Faculty of Electronic and Information Engineering, Xi'an Jiaotong University, Xi'an, Shaanxi, 710049, China.

REFERENCES

1. The 1000 Genomes Project Consortium (2010). A map of human genome variation from population-scale sequencing. Nature *467*, 1061–1073.

2. The 1000 Genomes Project Consortium (2012). An integrated map of genetic variation from

1,092 human genomes. Nature *491*, 56–65.

3. The 1000 Genomes Project Consortium (2015). A global reference for human genetic variation. Nature *526*, 68–74.

4. Sudmant, P.H., Rausch, T., Gardner, E.J., Handsaker, R.E., Abyzov, A., Huddleston, J., Zhang, Y., Ye, K., Jun, G., Fritz, M.H.-Y., et al. (2015). An integrated map of structural variation in 2,504 human genomes. Nature *526*, 75–81.

5. The International HapMap 3 Consortium (2010). Integrating common and rare genetic variation in diverse human populations. Nature *467*, 52.

6. Khurana, E., Fu, Y., Colonna, V., Mu, X.J., Kang, H.M., Lappalainen, T., Sboner, A., Lochovsky, L., Chen, J., Harmanci, A., et al. (2013). Integrative annotation of variants from 1092 humans: application to cancer genomics. Science *342*, 1235587.

7. Ritchie, G.R.S., Dunham, I., Zeggini, E., and Flicek, P. (2014). Functional annotation of noncoding sequence variants. Nat. Methods *11*, 294–296.

8. Kircher, M., Witten, D.M., Jain, P., O'Roak, B.J., Cooper, G.M., and Shendure, J. (2014). A general framework for estimating the relative pathogenicity of human genetic variants. Nat. Genet. *46*, 310–315.

9. Lappalainen, T., Sammeth, M., Friedländer, M.R., 't Hoen, P.A.C., Monlong, J., Rivas, M.A., Gonzàlez-Porta, M., Kurbatova, N., Griebel, T., Ferreira, P.G., et al. (2013). Transcriptome and genome sequencing uncovers functional variation in humans. Nature *501*, 506–511.

10. Huang, J., Chen, J., Esparza, J., Ding, J., Elder, J.T., Abecasis, G.R., Lee, Y.-A., Mark Lathrop, G., Moffatt, M.F., Cookson, W.O.C., et al. (2015). eQTL mapping identifies insertion- and deletion-specific eQTLs in multiple tissues. Nat. Commun. *6*, 6821.

11. Almeida, R., Ricaño-Ponce, I., Kumar, V., Deelen, P., Szperl, A., Trynka, G., Gutierrez-Achury, J., Kanterakis, A., Westra, H.-J., Franke, L., et al. (2014). Fine mapping of the celiac disease-associated LPP locus reveals a potential functional variant. Hum. Mol. Genet. *23*, 2481–2489.

12. Nikpay, M., Goel, A., Won, H.-H., Hall, L.M., Willenborg, C., Kanoni, S., Saleheen, D., Kyriakou, T., Nelson, C.P., Hopewell, J.C., et al. (2015). A comprehensive 1000 Genomes–based genome-wide association meta-analysis of coronary artery disease. Nat. Genet. *47*, 1121–1130.

13. Horikoshi, M., Mägi, R., van de Bunt, M., Surakka, I., Sarin, A.-P., Mahajan, A., Marullo, L., Thorleifsson, G., Hägg, S., Hottenga, J.-J., et al. (2015). Discovery and Fine-Mapping of Glycaemic and Obesity-Related Trait Loci Using High-Density Imputation. PLoS Genet. *11*, e1005230.

14. Hara, K., Fujita, H., Johnson, T.A., Yamauchi, T., Yasuda, K., Horikoshi, M., Peng, C., Hu, C., Ma, R.C.W., Imamura, M., et al. (2014). Genome-wide association study identifies three novel loci for type 2 diabetes. Hum. Mol. Genet. *23*, 239–246.

15. Zheng-Bradley, X., and Flicek, P. (2017). Applications of the 1000 Genomes Project resources. Brief. Funct. Genomics *16*, 163–170.

16. Eberle, M.A., Fritzilas, E., Krusche, P., Källberg, M., Moore, B.L., Bekritsky, M.A., Iqbal, Z., Chuang, H.-Y., Humphray, S.J., Halpern, A.L., et al. (2017). A reference data set of 5.4 million phased human variants validated by genetic inheritance from sequencing a three-generation 17-member pedigree. Genome Res. *27*, 157–164.

17. Chaisson, M.J.P., Sanders, A.D., Zhao, X., Malhotra, A., Porubsky, D., Rausch, T., Gardner, E.J., Rodriguez, O.L., Guo, L., Collins, R.L., et al. (2019). Multi-platform discovery of haplotype-resolved structural variation in human genomes. Nat. Commun. *10*, 1784.

18. Ebert, P., Audano, P.A., Zhu, Q., Rodriguez-Martin, B., Porubsky, D., Bonder, M.J., Sulovari, A., Ebler, J., Zhou, W., Mari, R.S., et al. (2020). De novo assembly of 64 haplotype-resolved human genomes of diverse ancestry and integrated analysis of structural variation. bioRxiv Doi: 10.1101/2020.12.16.423102.

19. Collins, R.L., Brand, H., Karczewski, K.J., Zhao, X., Alföldi, J., Francioli, L.C., Khera, A.V., Lowther, C., Gauthier, L.D., Wang, H., et al. (2020). A structural variation reference for medical and population genetics. Nature *581*, 444–451.

20. Abel, H.J., Larson, D.E., Regier, A.A., Chiang, C., Das, I., Kanchi, K.L., Layer, R.M., Neale, B.M., Salerno, W.J., Reeves, C., et al. (2020). Mapping and characterization of structural variation in 17,795 human genomes. Nature *583*, 83–89.

21. Karczewski, K.J., Francioli, L.C., Tiao, G., Cummings, B.B., Alföldi, J., Wang, Q., Collins, R.L., Laricchia, K.M., Ganna, A., Birnbaum, D.P., et al. (2020). The mutational constraint spectrum quantified from variation in 141,456 humans. Nature *581*, 434–443.

22. Taliun, D., Harris, D.N., Kessler, M.D., and Carlson, J. (2019). Sequencing of 53,831 diverse genomes from the NHLBI TOPMed Program. bioRxiv Doi: 10.1101/563866.

23. Regier, A.A., Farjoun, Y., Larson, D.E., Krasheninina, O., Kang, H.M., Howrigan, D.P., Chen, B.-J., Kher, M., Banks, E., Ames, D.C., et al. (2018). Functional equivalence of genome sequencing analysis pipelines enables harmonized variant calling across human genetics projects. Nat. Commun. *9*, 4038.

24. Zook, J.M., McDaniel, J., Olson, N.D., Wagner, J., Parikh, H., Heaton, H., Irvine, S.A., Trigg, L., Truty, R., McLean, C.Y., et al. (2019). An open resource for accurately benchmarking small variant and reference calls. Nat. Biotechnol. *37*, 561–566.

25. Campbell, M.C., and Tishkoff, S.A. (2008). African genetic diversity: implications for human demographic history, modern human origins, and complex disease mapping. Annu. Rev. Genomics Hum. Genet. *9*, 403–433.

26. Updated GRCh38 liftover of the 1000 Genomes Project phase 3 call set: https://www.internationalgenome.org/announcements/updated-GRCh38-liftover/.

27. Database of Single Nucleotide Polymorphisms (dbSNP). Bethesda (MD): National Center for Biotechnology Information, National Library of Medicine. (dbSNP Build ID: 149). Available from:

http://www.ncbi.nlm.nih.gov/SNP/.

28. Delaneau, O., Marchini, J., and Zagury, J.-F. (2011). A linear complexity phasing method for thousands of genomes. Nat. Methods *9*, 179–181.

29. O'Connell, J., Gurdasani, D., Delaneau, O., Pirastu, N., Ulivi, S., Cocca, M., Traglia, M., Huang, J., Huffman, J.E., Rudan, I., et al. (2014). A general approach for haplotype phasing across the full spectrum of relatedness. PLoS Genet. *10*, e1004234.

30. Loh, P.-R., Danecek, P., Palamara, P.F., Fuchsberger, C., A Reshef, Y., K Finucane, H., Schoenherr, S., Forer, L., McCarthy, S., Abecasis, G.R., et al. (2016). Reference-based phasing using the Haplotype Reference Consortium panel. Nat. Genet. *48*, 1443–1448.

31. Wigginton, J.E., Cutler, D.J., and Abecasis, G.R. (2005). A note on exact tests of Hardy-Weinberg equilibrium. Am. J. Hum. Genet. *76*, 887–893.

32. Mallick, S., Li, H., Lipson, M., Mathieson, I., Gymrek, M., Racimo, F., Zhao, M., Chennagiri, N., Nordenfelt, S., Tandon, A., et al. (2016). The Simons Genome Diversity Project: 300 genomes from 142 diverse populations. Nature *538*, 201–206.

33. Howie, B.N., Donnelly, P., and Marchini, J. (2009). A flexible and accurate genotype imputation method for the next generation of genome-wide association studies. PLoS Genet. *5*, e1000529.

34. Polaris: https://github.com/Illumina/Polaris/tree/master/cohorts/1000_genomes.

35. Poplin, R., Ruano-Rubio, V., DePristo, M.A., Fennell, T.J., Carneiro, M.O., Van der Auwera, G.A., Kling, D.E., Gauthier, L.D., Levy-Moonshine, A., Roazen, D., et al. (2017). Scaling accurate genetic variant discovery to tens of thousands of samples. bioRxiv Doi: 10.1101/201178 201178.

36. Cingolani, P., Platts, A., Wang, L.L., Coon, M., Nguyen, T., Wang, L., Land, S.J., Lu, X., and Ruden, D.M. (2012). A program for annotating and predicting the effects of single nucleotide polymorphisms, SnpEff: SNPs in the genome of Drosophila melanogaster strain w1118; iso-2; iso-3. Fly *6*, 80–92.

37. Li, H. (2011). A statistical framework for SNP calling, mutation discovery, association mapping and population genetical parameter estimation from sequencing data. Bioinformatics *27*, 2987–2993.

38. Tate, J.G., Bamford, S., Jubb, H.C., Sondka, Z., Beare, D.M., Bindal, N., Boutselakis, H., Cole, C.G., Creatore, C., Dawson, E., et al. (2019). COSMIC: the Catalogue Of Somatic Mutations In Cancer. Nucleic Acids Res. *47*, D941–D947.

39. Liu, X., Jian, X., and Boerwinkle, E. (2011). dbNSFP: a lightweight database of human nonsynonymous SNPs and their functional predictions. Hum. Mutat. *32*, 894–899.

40. Liu, X., Wu, C., Li, C., and Boerwinkle, E. (2016). DbNSFP v3.0: A one-stop database of functional predictions and annotations for human nonsynonymous and splice-site SNVs. Hum. Mutat. *37*, 235–241.

41. Lek, M., Karczewski, K.J., Minikel, E.V., Samocha, K.E., Banks, E., Fennell, T., O'Donnell-Luria, A.H., Ware, J.S., Hill, A.J., Cummings, B.B., et al. (2016). Analysis of protein-coding genetic variation in 60,706 humans. Nature *536*, 285–291.

42. Jun, G., Flickinger, M., Hetrick, K.N., Romm, J.M., Doheny, K.F., Abecasis, G.R., Boehnke, M., and Kang, H.M. (2012). Detecting and Estimating Contamination of Human DNA Samples in Sequencing and Array-Based Genotype Data. The American Journal of Human Genetics *91*, 839–848.

43. Cleary, J.G., Braithwaite, R., Gaastra, K., Hilbush, B.S., Inglis, S., Irvine, S.A., Jackson, A., Littin, R., Rathod, M., Ware, D., et al. (2015). Comparing Variant Call Files for Performance Benchmarking of Next-Generation Sequencing Variant Calling Pipelines. bioRxiv Doi: 10.1101/023754 023754.

44. Zhao, H., Sun, Z., Wang, J., Huang, H., Kocher, J.-P., and Wang, L. (2014). CrossMap: a versatile tool for coordinate conversion between genome assemblies. Bioinformatics *30*, 1006–1007.

45. Werling, D.M., Brand, H., An, J.-Y., Stone, M.R., Zhu, L., Glessner, J.T., Collins, R.L., Dong, S., Layer, R.M., Markenscoff-Papadimitriou, E., et al. (2018). An analytical framework for whole-genome sequence association studies and its implications for autism spectrum disorder. Nat. Genet. *50*, 727–736.

46. Larson, D.E., Abel, H.J., Chiang, C., Badve, A., Das, I., Eldred, J.M., Layer, R.M., and Hall, I.M. (2019). svtools: population-scale analysis of structural variation. Bioinformatics *35*, 4782–4787.

47. Layer, R.M., Chiang, C., Quinlan, A.R., and Hall, I.M. (2014). LUMPY: a probabilistic framework for structural variant discovery. Genome Biol. *15*, R84.

48. Chen, X., Schulz-Trieglaff, O., Shaw, R., Barnes, B., Schlesinger, F., Källberg, M., Cox, A.J., Kruglyak, S., and Saunders, C.T. (2016). Manta: rapid detection of structural variants and indels for germline and cancer sequencing applications. Bioinformatics *32*, 1220–1222.

49. Chiang, C., Layer, R.M., Faust, G.G., Lindberg, M.R., Rose, D.B., Garrison, E.P., Marth, G.T., Quinlan, A.R., and Hall, I.M. (2015). SpeedSeq: ultra-fast personal genome analysis and interpretation. Nat. Methods *12*, 966–968.

50. Abyzov, A., Urban, A.E., Snyder, M., and Gerstein, M. (2011). CNVnator: an approach to discover, genotype, and characterize typical and atypical CNVs from family and population genome sequencing. Genome Res. *21*, 974–984.

51. Chen, S., Krusche, P., Dolzhenko, E., Sherman, R.M., Petrovski, R., Schlesinger, F., Kirsche, M., Bentley, D.R., Schatz, M.C., Sedlazeck, F.J., et al. (2019). Paragraph: a graph-based structural variant genotyper for short-read sequence data. Genome Biol. *20*, 291.

52. Katoh, K., and Standley, D.M. (2013). MAFFT multiple sequence alignment software version 7: improvements in performance and usability. Mol. Biol. Evol. *30*, 772–780.

53. Zhao, X., Weber, A.M., and Mills, R.E. (2017). A recurrence-based approach for validating

structural variation using long-read sequencing technology. Gigascience *6*, 1–9.

54. Ke, G., Meng, Q., Finley, T., Wang, T., Chen, W., Ma, W., Ye, Q., and Liu, T.-Y. (2017). LightGBM: A Highly Efficient Gradient Boosting Decision Tree. In Advances in Neural Information Processing Systems 30, I. Guyon, U.V. Luxburg, S. Bengio, H. Wallach, R. Fergus, S. Vishwanathan, and R. Garnett, eds. (Curran Associates, Inc.), pp. 3146–3154.

55. Martin, M., Patterson, M., Garg, S., Fischer, S.O., Pisanti, N., Klau, G.W., Schöenhuth, A., and Marschall, T. (2016). WhatsHap: fast and accurate read-based phasing. bioRxiv 085050.

56. Purcell, S., Neale, B., Todd-Brown, K., Thomas, L., Ferreira, M.A.R., Bender, D., Maller, J., Sklar, P., de Bakker, P.I.W., Daly, M.J., et al. (2007). PLINK: a tool set for whole-genome association and population-based linkage analyses. Am. J. Hum. Genet. *81*, 559–575.

FIGURES

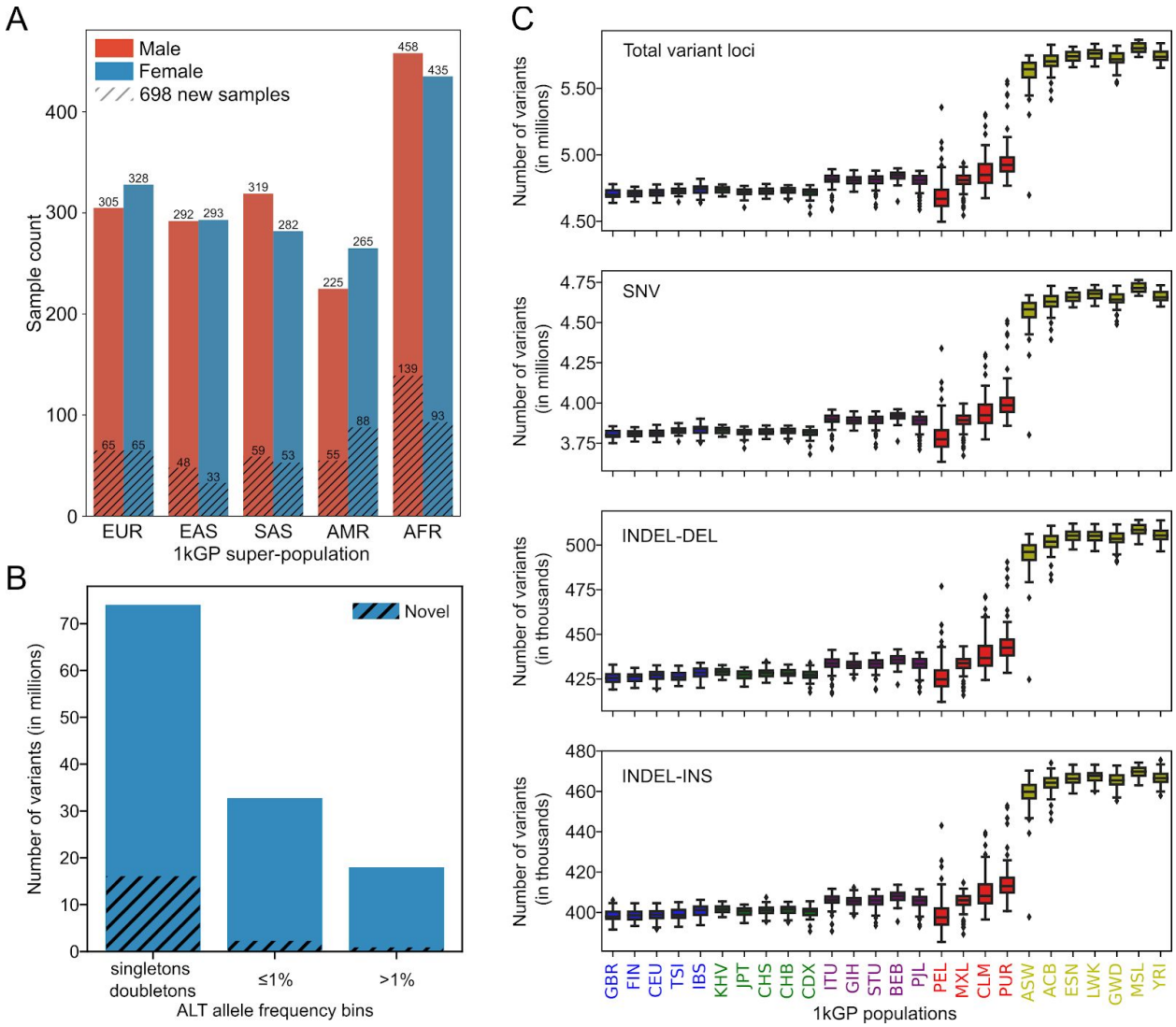

Figure 1. SNV/INDEL discovery across the 3,202 1kGP samples in high coverage WGS data. A) Sample counts per super-population stratified by sex. Shaded areas represent counts coming from the newly added 698 related samples. **B)** SNV/INDEL counts, stratified by AF bins (unrelated samples only). Counts of variants with AC=1 or AC=2 (singletons and doubletons) are reported as a separate bin and were excluded from the ≤1% AF bin. **C)** Number of small variant loci per genome, stratified by population. From top to bottom: total count of variant loci, counts of single nucleotide variants (SNV), count of small deletions, count of small insertions. Complex variants and MNPs were not included in the breakdown. In all panels, counts are restricted to variants that passed VQSR. Color labels along the x axis correspond to the following super-populations: blue: EUR, green: EAS, purple: SAS, red: AMR, yellow: AFR.

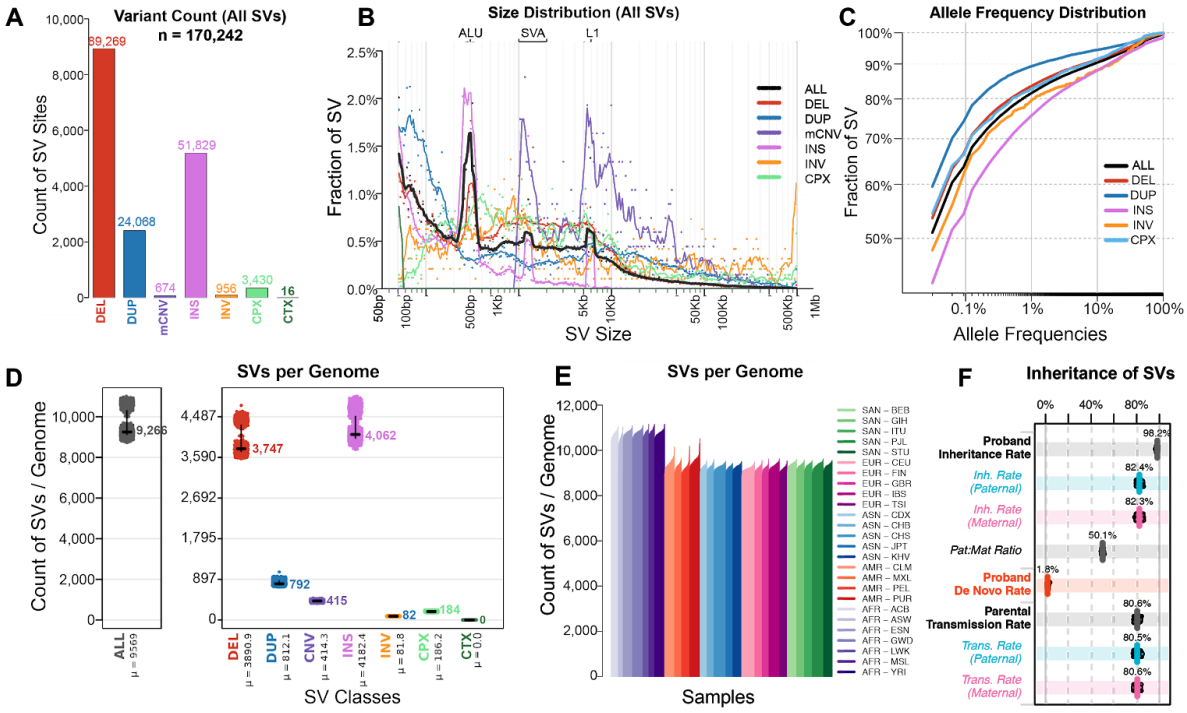

Figure 2. Overview of the 1000 Genomes SV callset. A) The count, **(B)** size distribution, and **(C)** allele frequency distribution of each SV for each SV class is shown. The per sample counts of SVs by variant class **(D)** and ancestral population **(E)** is also provided, as well as **(F)** inheritance rates of all SVs.

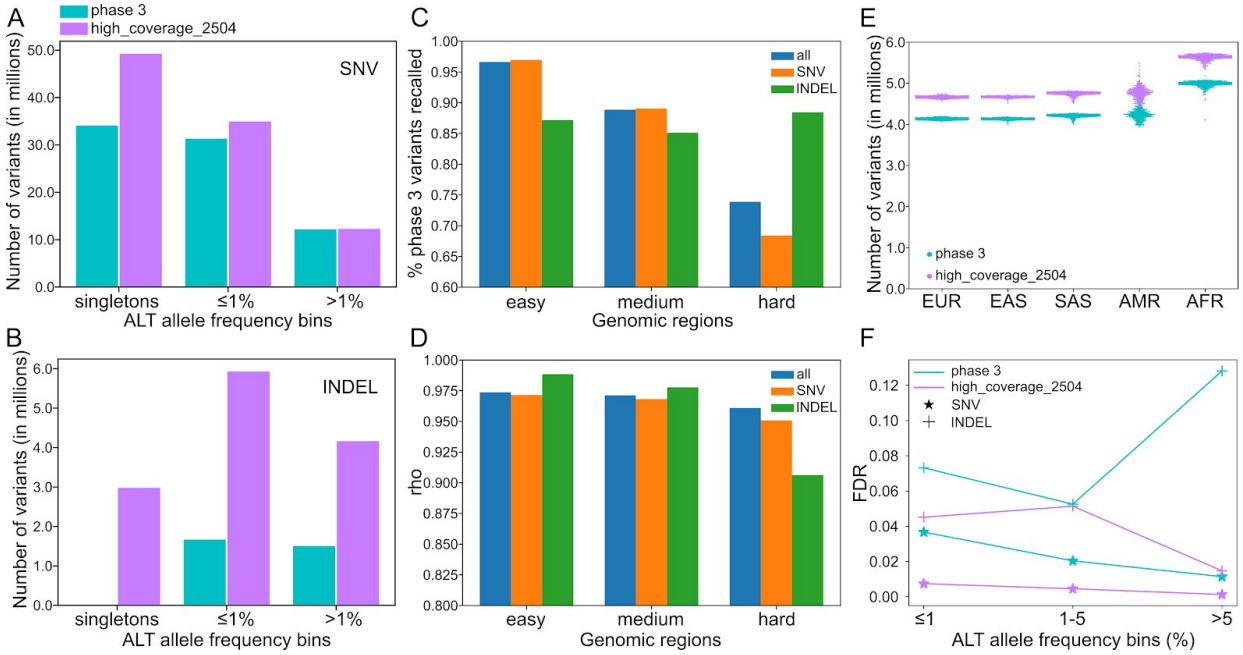

Figure 3. Comparison of autosomal SNV and INDEL calls between the high coverage and the phase 3 1kGP callsets. For consistency, the high coverage dataset was restricted to the 2,504 samples that are shared between the two callsets. Number of SNVs **(A)** and INDELs **(B)** across the 2,504 samples in phase 3 (aqua) and high coverage (purple) datasets, stratified by AF bins. Counts of variants with AC=1 (singletons) are reported as a separate bin and were excluded from the ≤1% AF bin. Multiallelic loci were split into separate lines and INDEL representation was normalized prior to counting, *i.e.* the reported counts are at the alternate allele (as opposed to locus) level. **(C)** Percent of phase 3 variants recalled in the high coverage dataset stratified by variant type (blue: all, orange: SNVs, green: INDELs) and regions of the genome (easy: regions where we can confidently call variants, medium: regions that did not fall in either easy or hard category, hard: centromeres, repetitive and low complexity regions). **(D)** Correlation of non-reference allele frequency of shared variants in the high coverage vs. phase 3 callsets, stratified by easy, medium, hard regions of the genome, as defined in C. Plotted on y-axis is the spearman correlation coefficient (rho). **(E)** Total number of SNV and INDEL loci per genome in the phase 3 (aqua) and the high coverage (purple) dataset, stratified by 1kGP super-populations. **(F)** Comparison of FDR between the high coverage (purple) and phase 3 (aqua) callsets across AF bins, stratified by variant type (star: SNV, plus sign: INDEL).

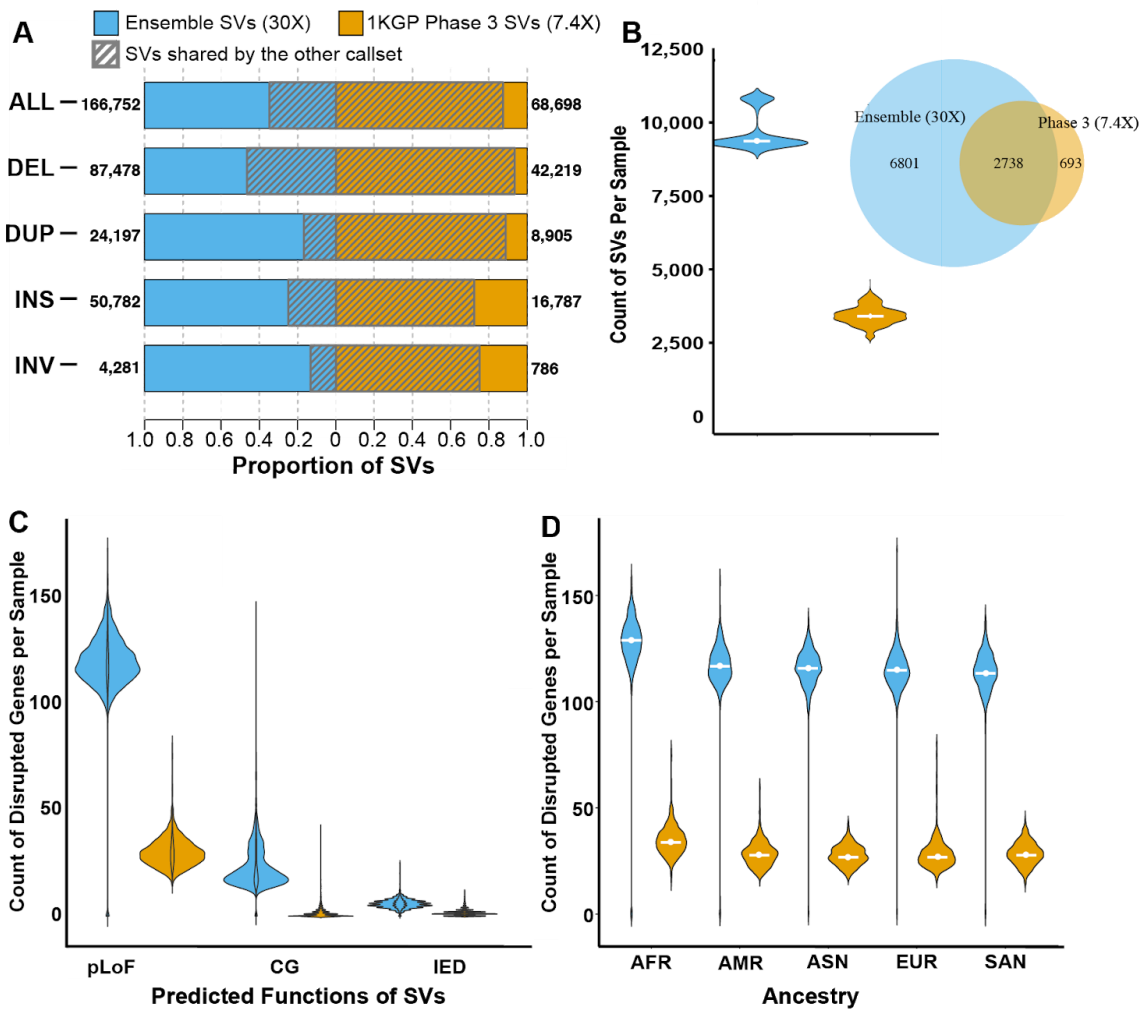

Figure 4. Comparison of high-coverage ensemble SV callset to low-coverage phase 3 SV callset. (A) Count of SV sites in the current ensemble SV callset and low-coverage phase 3 SV callset, and their overlap. Numbers next to each bar represent the counts of SV sites in each dataset. **(B)** The distribution of SVs counts per sample in both callsets, and their average overlap displayed in the venn diagram. **(C)** Count of genes altered by SVs in both datasets. pLoF: probable loss of function, CG: complete copy gain, IED: intragenic exon duplication. **(D)** Count of genes altered by pLoF SVs across ancestral populations.

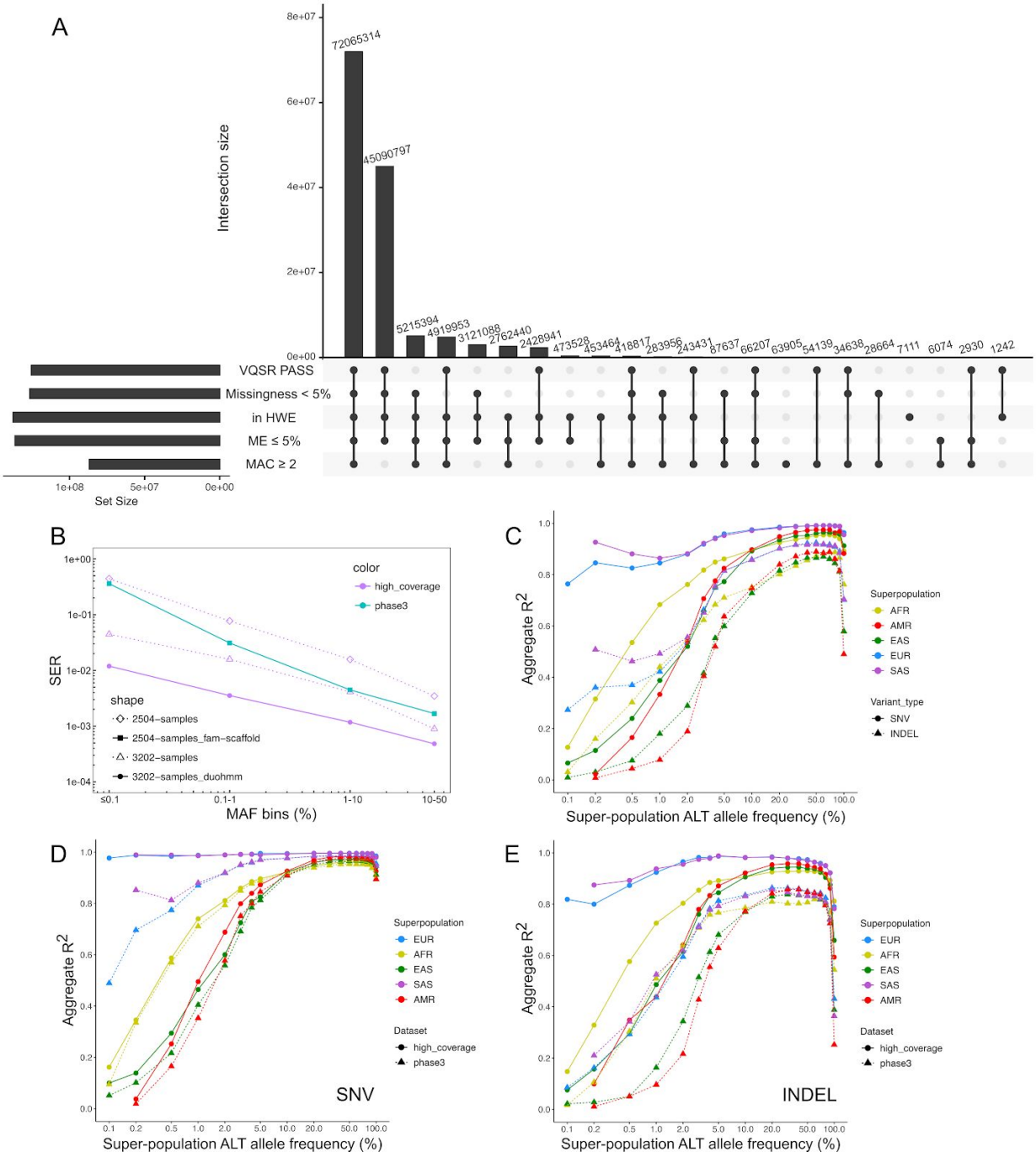

Figure 5. SNV/INDEL phasing and imputation performance evaluation. A) Counts of SNVs/INDELs meeting specified filtering criteria. Multiallelic variants were split into separate rows prior to counting. HWE: HWE exact test p-value > 1e-10 in at least one of the 5 super-populations (EUR, AFR, EAS, SAS, AMR); ME: mendelian error among complete trios (*i.e.* trios where all family members have a called GT at a given site); MAC: minor allele count. The set of SNV/INDELs meeting all 5 QC criteria (first bar from the left) was selected for haplotype phasing. See Figure S5 for a similar plot stratified by variant type. **B)** Haplotype phasing accuracy evaluation of the high coverage (purple) vs. the phase 3 (aqua) 1kGP

SNV/INDEL panel. Switch error rate (SER) was computed across all pairs of consecutive heterozygous SNV/INDELs in specified MAF bins for sample NA12878, using the Platinum Genome NA12878 callset as gold standard truth set (autosomes only). Three phasing conditions applied to the high coverage dataset (purple): (1) solid line with circles: 3,202-sample panel phased using statistical phasing with pedigree-based correction; (2) dashed line with triangles: 3,202-sample panel phased using statistical phasing *without* pedigree-based correction; (3) dashed line with diamonds: 2,504-sample panel phased using statistical phasing (unrelated samples only). The 2 panels represented with dashed lines were created for evaluation purposes only. Aqua solid line with squares: 2,504-sample phase 3 SNV/INDEL panel phased using statistical phasing with family-based scaffold. **C)** Imputation accuracy of SNV (solid lines with circles) and INDEL (dashed lines with triangles) genotypes as a function of non-reference allele frequency in a given 1kGP super-population (blue: EUR, green: EAS, purple: SAS, red: AMR, yellow: AFR), achieved using the complete high coverage panel. Imputation accuracy is measured by the aggregate squared correlation (R^2) between imputed dosages and WGS dosages of the Simons Genome Diversity Project samples (average across 22 samples per super-population). Comparison of the imputation performance between the high coverage (solid lines with circles) and phase 3 (dashed lines with triangles) panels for SNVs **(D)** and INDELs **(E)**, stratified by super-population (the same colors as in C). Comparison in (D) and (E) was restricted to sites that are shared between the phase 3 and the high coverage panels (unlike panel C which shows performance across all sites for the high coverage panel).

SUPPLEMENTARY INFORMATION

Supplementary Figures.

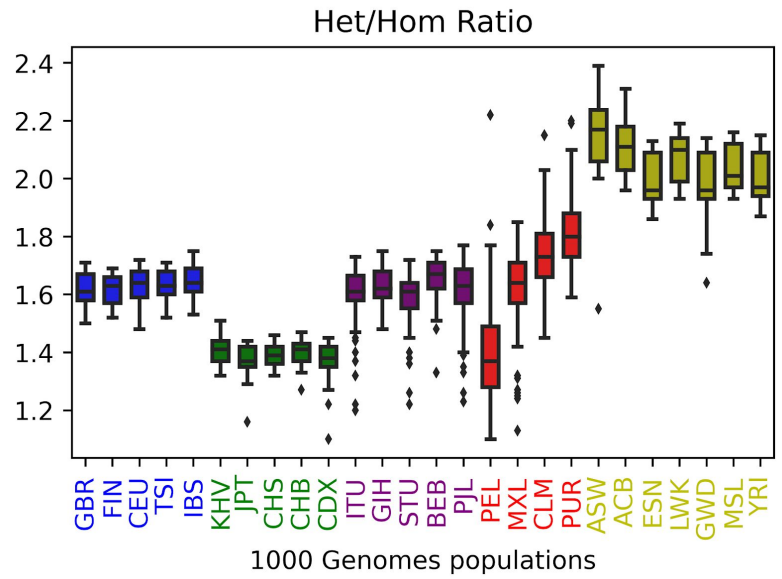

Figure S1. Distribution of per sample heterozygous to homozygous ratio (Het/Hom) based on SNVs and INDELs across the 3,202 samples.

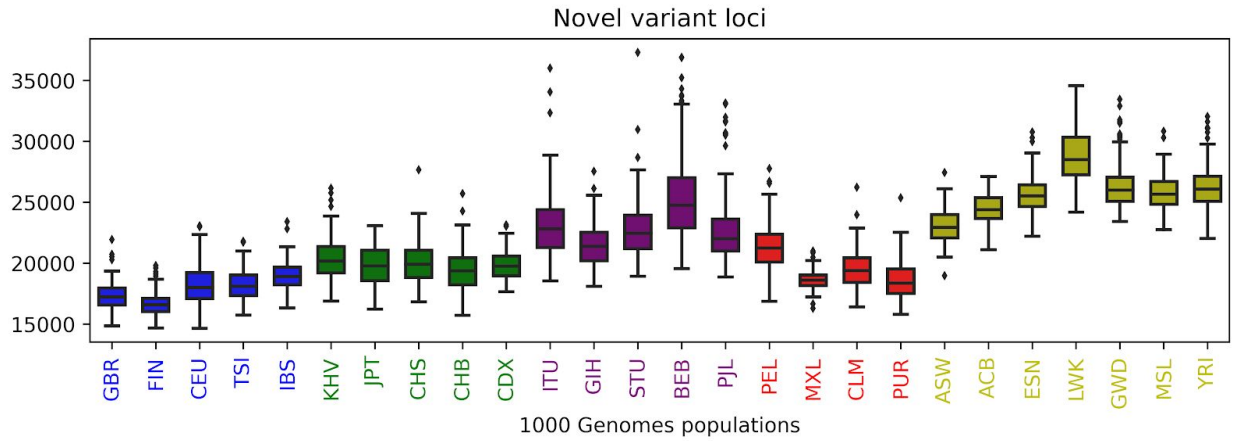

Figure S2. Counts of novel variants across all populations. Novel variants are defined as variants that are not reported in dbSNP build 151.

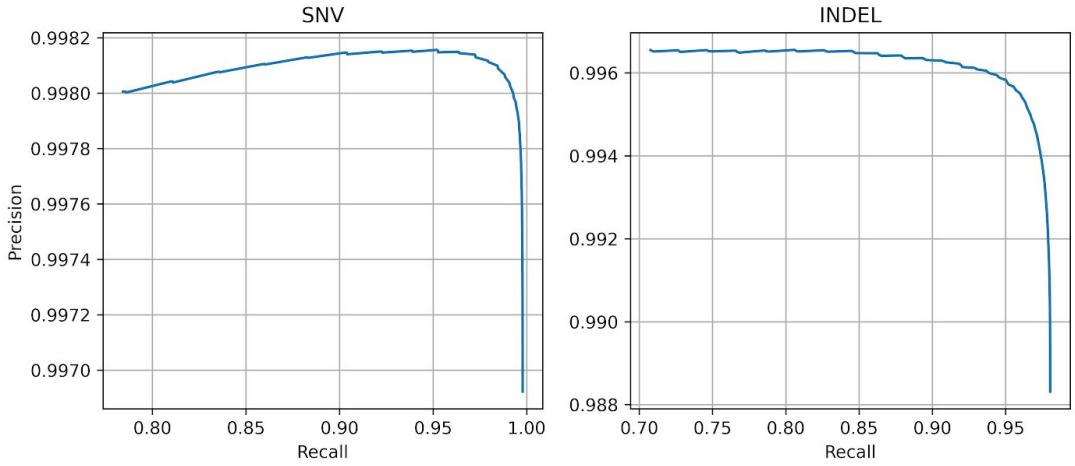

Figure S3. Sensitivity vs. precision of SNV/INDEL calls in the high coverage 3,202-sample callset, based on comparison against the GIAB NA12878 truth set.

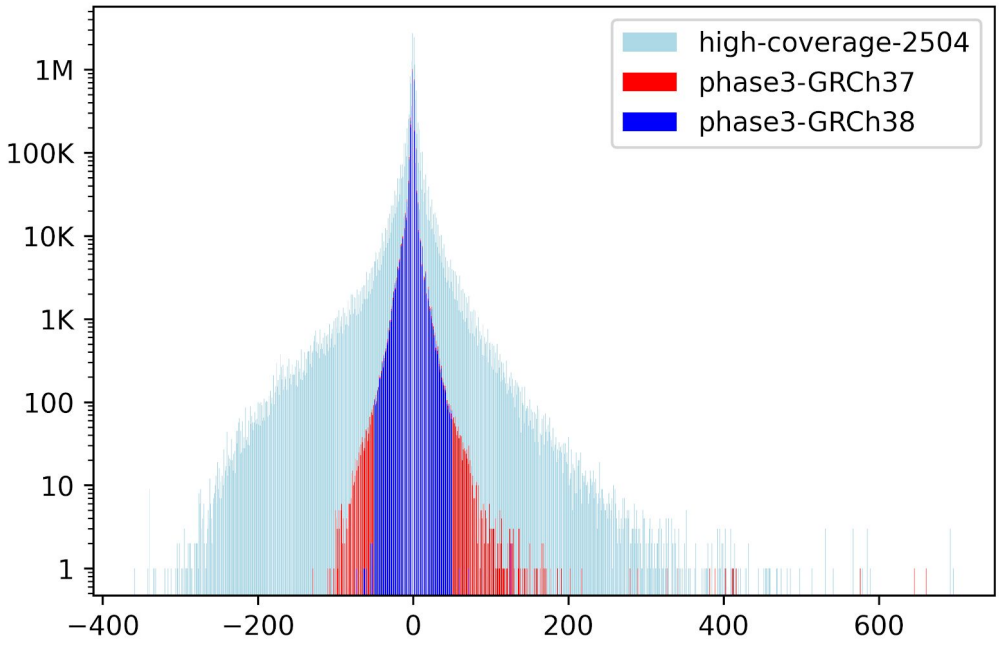

Figure S4. Length distribution of INDEL calls in the 2,504-sample high coverage and phase 3 callsets.

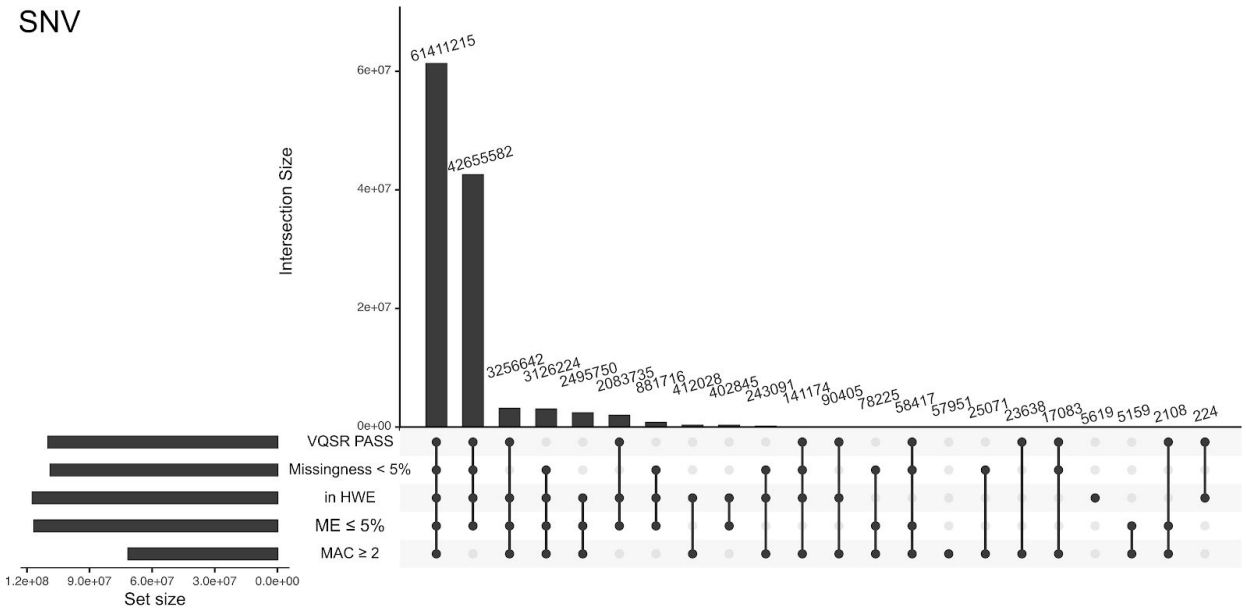
SNV
Intersection Size
6e+07
4e+07
2e+07
0e+00
61411215
42655582
3256642
3126224
2495750
2083735
881716
412028
402845
243091
141174
90405
78225
58417
57951
25071
23638
17083
5619
5159
2108
224
VQSR PASS
Missingness < 5%
in HWE
ME ≤ 5%
MAC ≥ 2
1.2e+08
9.0e+07
6.0e+07
3.0e+07
0.0e+00
Set size

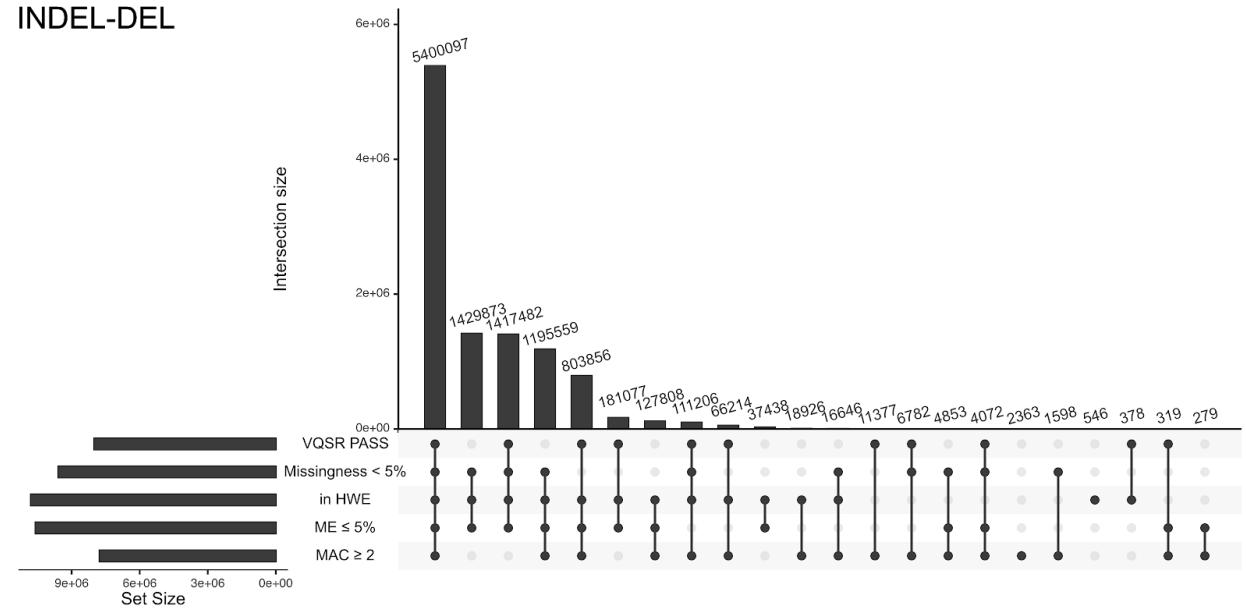
INDEL-DEL
Intersection size
6e+06
4e+06
2e+06
0e+00
5400097
1429873
1417482
1195559
803856
181077
127808
111206
66214
37438
18926
16646
11377
6782
4853
4072
2363
1598
546
378
319
279
VQSR PASS
Missingness < 5%
in HWE
ME ≤ 5%
MAC ≥ 2
9e+06
6e+06
3e+06
0e+00
Set Size

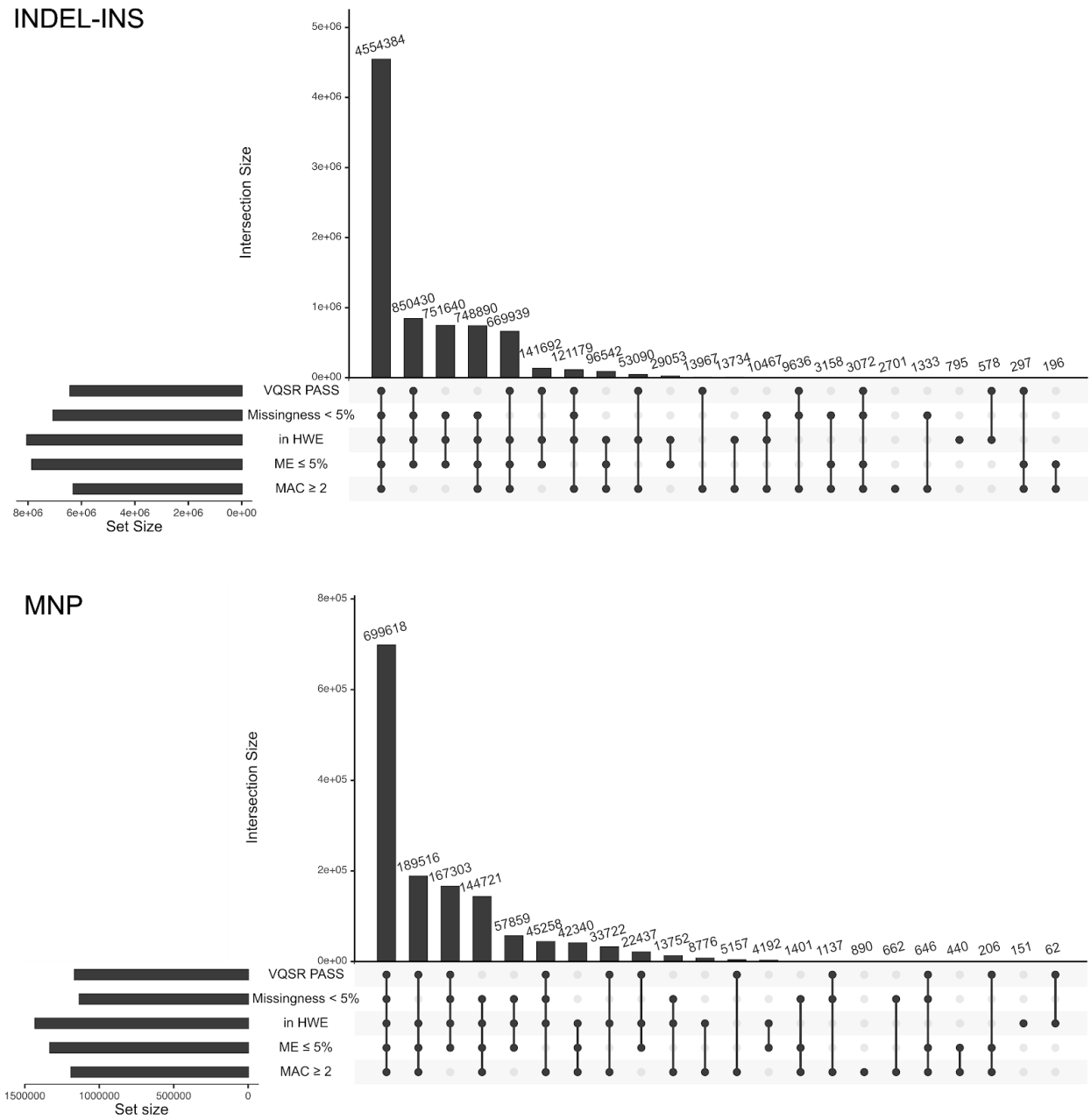

Figure S5. Counts of SNV/INDELs meeting specified filtering criteria stratified by variant type. Same as Figure 5A, but stratified by variant type.

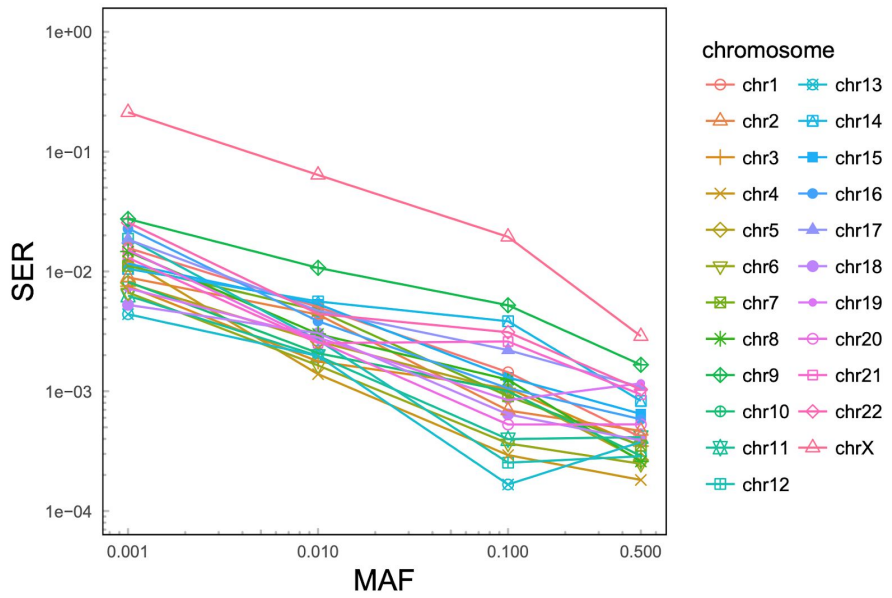

Figure S6. Phasing accuracy of the high coverage panel stratified by chromosome. Analogous to Figure 5B (solid purple line), but stratified by chromosome.

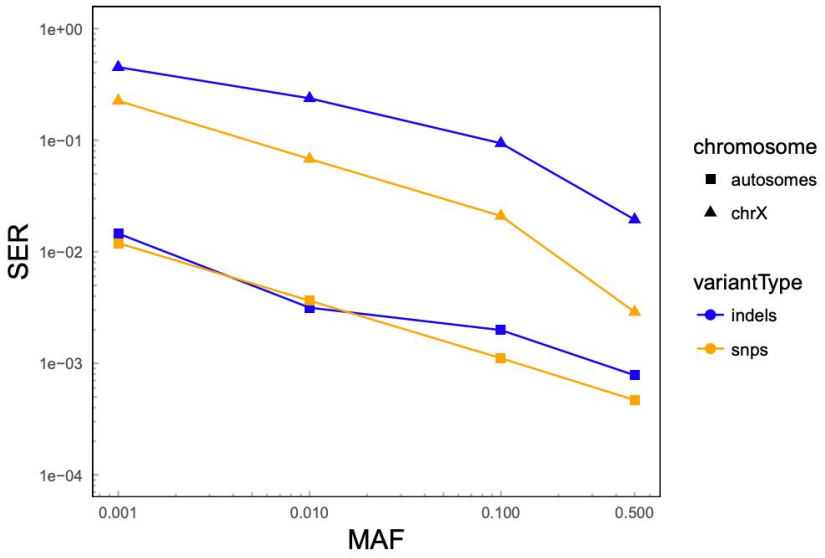

Figure S7. Phasing accuracy of the high coverage panel stratified by variant type. Chromosome X is shown separately as it was phased using a different strategy as compared to autosomes (statistical phasing vs. statistical phasing with pedigree-based correction, respectively).

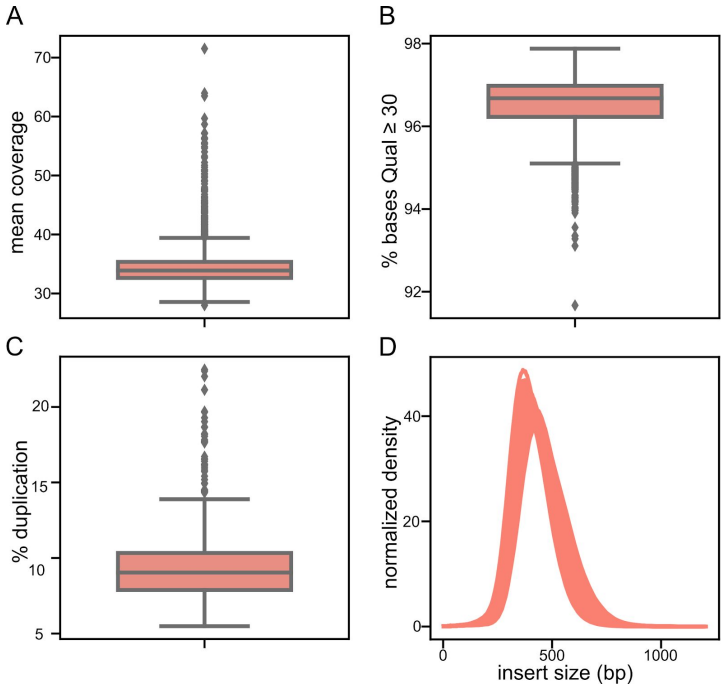

Figure S8. Per sample alignment metrics across the 3,202 1kGP samples. A) Mean coverage distribution. B) % bases with quality >= 30. C) % duplication. D) Insert size distribution.

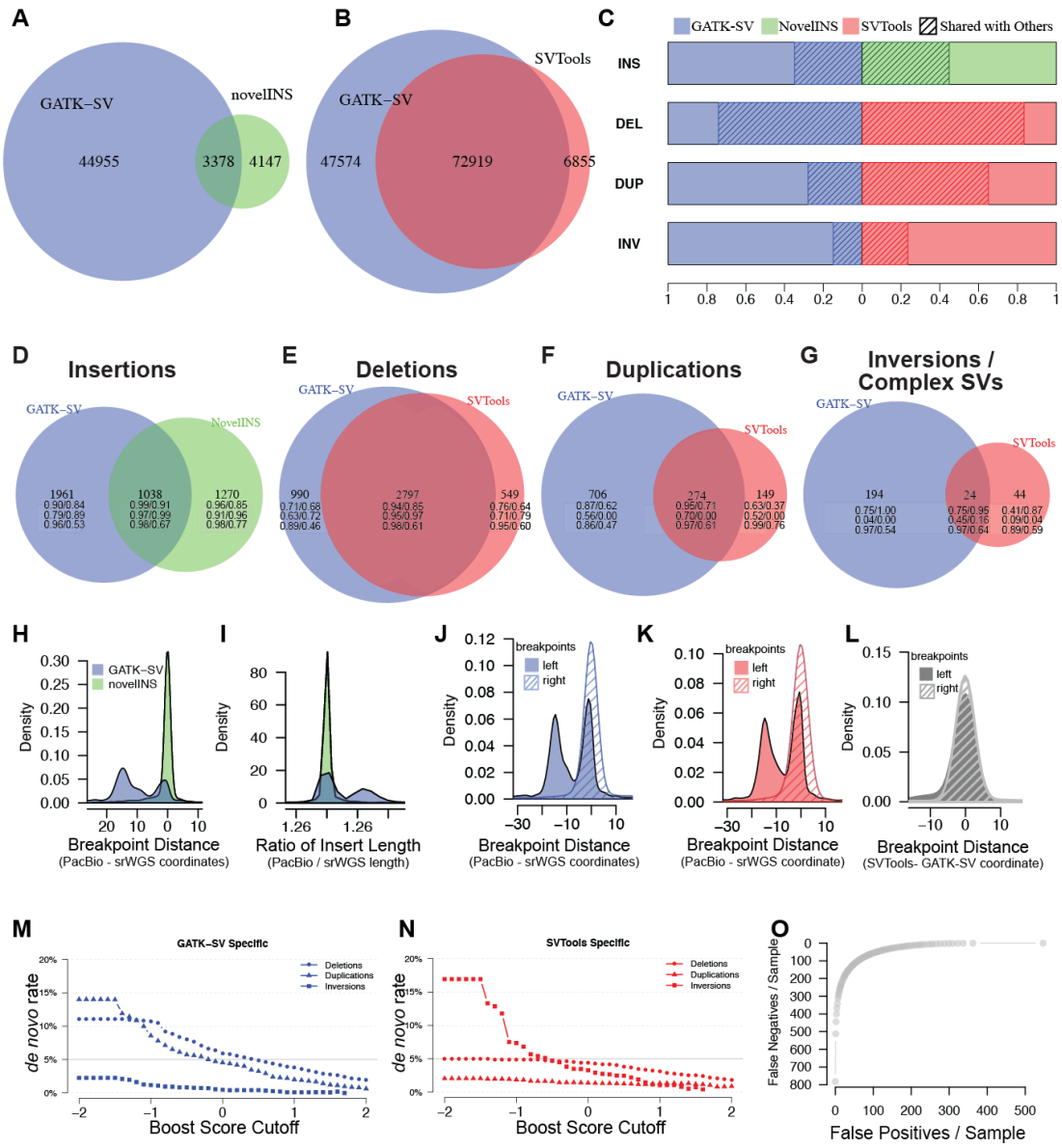

Figure S9. Benchmark of GATK-SV, svtools, and Absinthe. (A) Overlap of insertion sites between GAKT-SV and Absinthe callsets. (B) Overlap of SV other than insertions between the GATK-SV and svtools callset. (C) Overlap of each SV type between GATK-SV, svtools and Absinthe. (D) Overlap of insertions in each genome between GATK-SV and Absinthe. (E-G) Overlap of deletions (E), duplications (F), inversion and complex SVs (G) in each genome between GATK-SV and svtools. The integers in (D-G) represent count of SVs per sample, followed by proportion of SVs validated by VaPoR / proportion of SVs assessable by VaPoR in the second row, proportion of SVs supported by PacBio SVs in Ebert et al. 2020 / proportion of SVs supported by PacBio SVs in Chaisson *et al.* 2019 in the third row, and transmission rate /rate of bi-parentally inherited SVs in the fourth row. (H-I) Precision of the insertion breakpoint (H) and length (I) assessed against PacBio assemblies. (J-K) Precision of the SV breakpoints in GATK-SV (J) and svtools (K) callsets assessed against PacBio assemblies. (L) Breakpoint distance of SVs shared by GATK-SV and svtools. (M-N) *de novo* rate of SVs in GATK-SV (M)

and svtools (N) callset when filtered at different boost score cutoffs. (O) False positives and false negatives in the GATK-SV and svtools callsets when filtered at different boost score cutoffs.

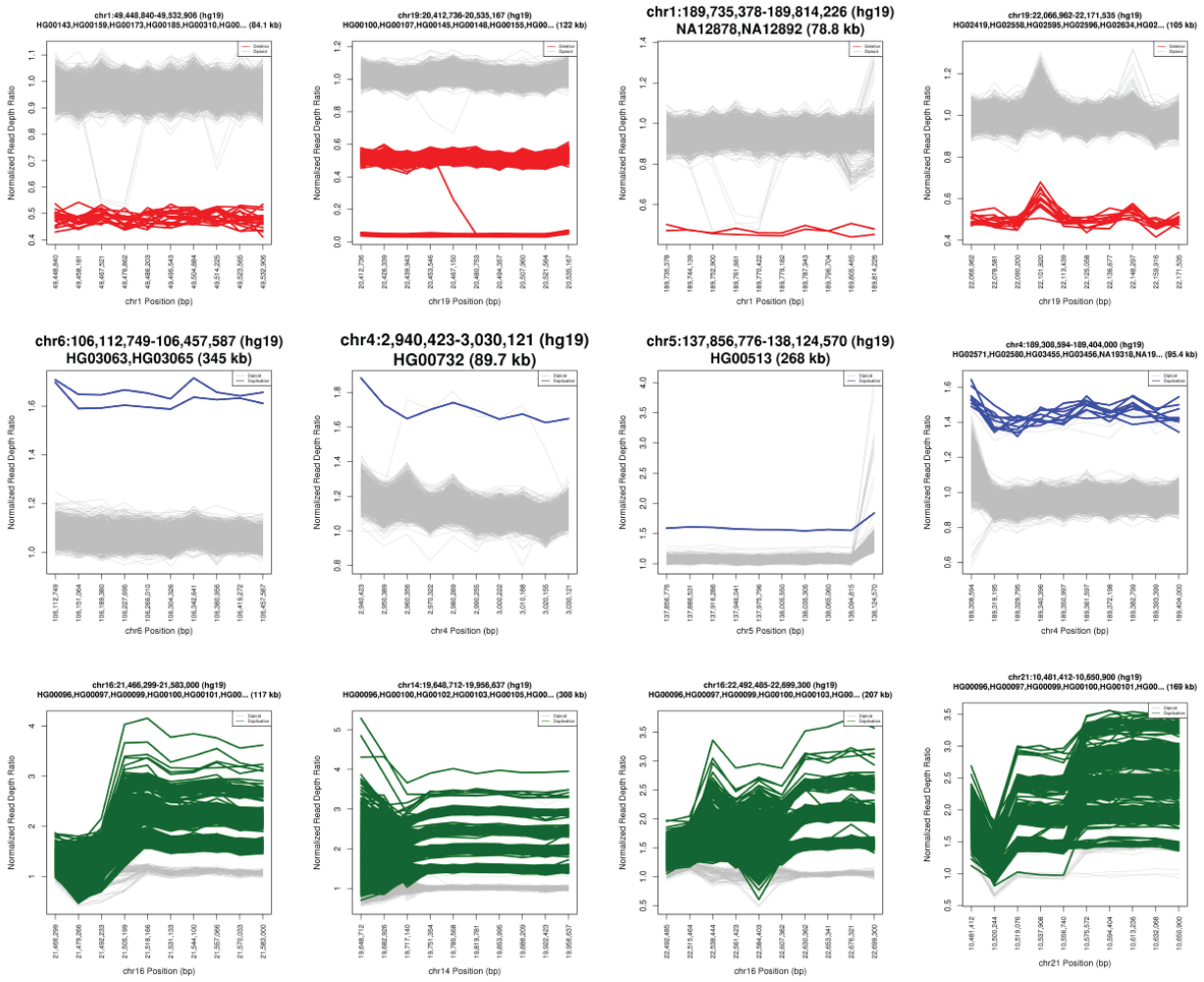

Figure S10. Read depth distribution of large deletions (red), duplications (blue) and multiallelic CNVs (green) across the 3,202 samples.

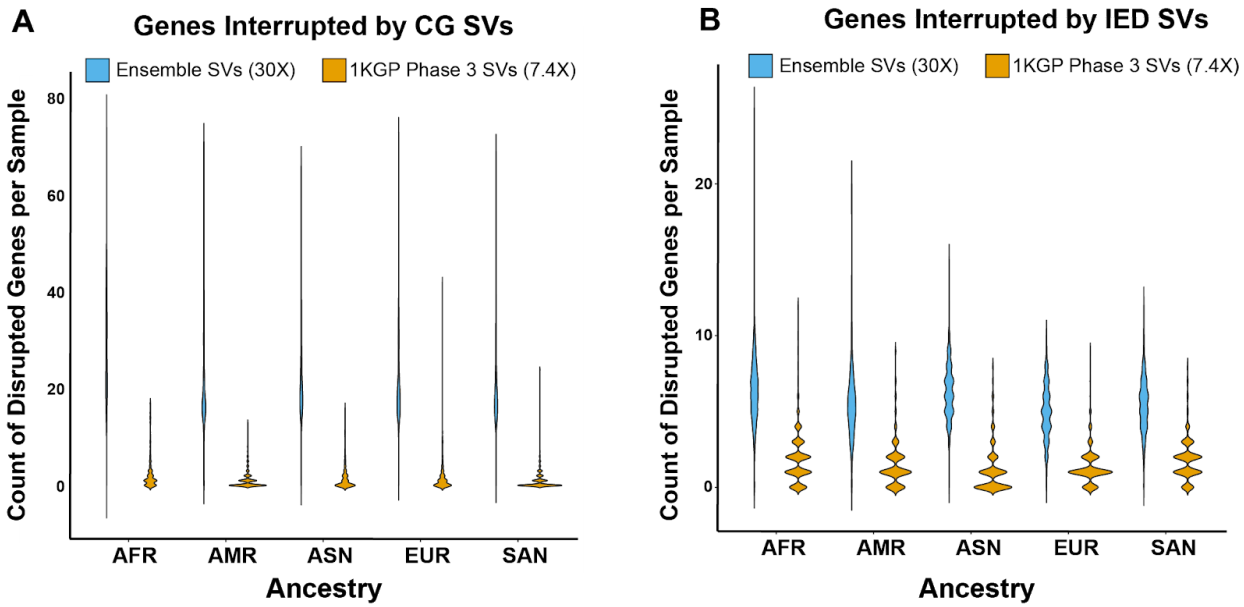

Figure S11. Count of genes interrupted by copy gain (GC) and interagenic exon duplications (IED) SVs in the current ensemble callset and 1kGP Phase 3 SV callset.

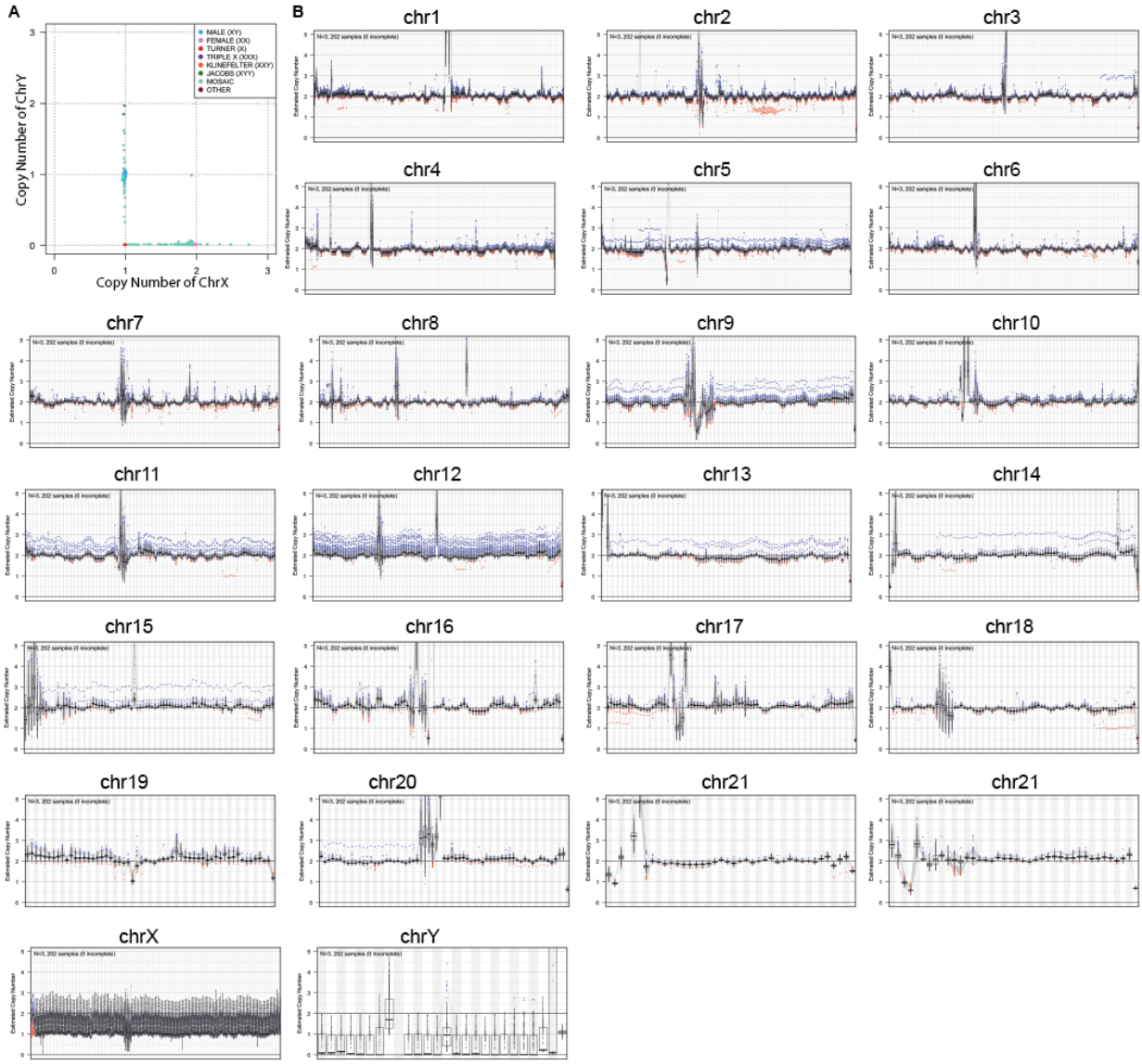

Figure S12. Ploidy of each chromosome across the 3,202 samples. (A). Ploidy of allosomes. (B). Copy number of each chromosome. Each dot represents a copy number of the 1Mbp bin in a sample. Blue dots are samples with copy gain and red dots represent copy loss.

Supplementary tables.

Table S1. Sample counts broken down by ancestry, sex, cohort, and presence within pedigrees.

Population	Super-population	Sex (1=male, 2=female)	Count in 3202-sample cohort	Count in 2504-sample cohort	Count of samples that are in trios	No. of trios
ACB	AFR	1	57	47	30	20
		2	59	49	30	
ASW	AFR	1	33	26	20	13
		2	41	35	19	
ESN	AFR	1	84	53	71	43
		2	65	46	58	
GWD	AFR	1	93	55	91	58
		2	85	58	83	
LWK	AFR	1	44	44	0	0
		2	55	55	0	
MSL	AFR	1	50	42	16	11
		2	49	43	17	
YRI	AFR	1	97	52	92	56
		2	81	56	76	
CLM	AMR	1	58	43	48	35
		2	74	51	57	
MXL	AMR	1	43	32	40	32
		2	54	32	50	
PEL	AMR	1	54	41	47	35
		2	68	44	58	
PUR	AMR	1	70	54	51	35
		2	69	50	54	
CDX	EAS	1	44	44	0	0
		2	49	49	0	
CHB	EAS	1	46	46	0	0
		2	57	57	0	

CHS	EAS	1	86	52	80	51
		2	77	53	70	
JPT	EAS	1	56	56	0	0
		2	48	48	0	
KHV	EAS	1	60	46	34	21
		2	62	53	29	
CEU	EUR	1	87	49	84	57
		2	92	50	87	
FIN	EUR	1	38	38	0	0
		2	61	61	0	
GBR	EUR	1	46	46	0	0
		2	45	45	0	
IBS	EUR	1	81	54	77	50
		2	76	53	73	
TSI	EUR	1	53	53	0	0
		2	54	54	0	
BEB	SAS	1	60	42	41	30
		2	71	44	49	
GIH	SAS	1	56	56	0	0
		2	47	47	0	
ITU	SAS	1	61	59	4	3
		2	46	43	5	
PJL	SAS	1	77	48	65	42
		2	69	48	61	
STU	SAS	1	65	55	16	10
		2	49	47	10	
Total:			3202	2504	1793	602

13 samples are part of 2 trios (hence only 1,793 unique samples contribute to the 602 trios; not 1,806), either because they are part of a multi-generational family, *i.e.* are a child in one trio and a parent in another trio (HG00702, NA19685, NA19675), and/or because they are a part of a quad (5 quads were included in total) that was broken down into 2 trios when pedigree-based correction was applied following haplotype phasing (HG00656, HG00657, HG03642, HG03679, HG03943, HG03944, NA19660, NA19661, NA19678, NA19679).

Table S2. Mean SNV density per 1kb of sequence in 3,202-sample high coverage callset.

	SNV Density per 1kb region	
Chromosome	Phased	Genotyped
chr1	21.88	36.46
chr2	23.89	40.16
chr3	23.89	40.11
chr4	24.39	41.3
chr5	23.76	39.91
chr6	23.99	39.88
chr7	24.61	41.1
chr8	25.5	42.84
chr9	21.76	36.66
chr10	24.77	41.15
chr11	24.11	40.61
chr12	23.65	39.82
chr13	24.22	41.04
chr14	23.93	40.06
chr15	23.52	39.21
chr16	24.78	41.43
chr17	23.39	39.02
chr18	23.25	39.6
chr19	26.62	43.21
chr20	24.23	40.34
chr21	22.84	37.77
chr22	25.03	41.41
chrX	17.04	30.16

Phased: SNV density in the phased high quality subset of SNV/INDEL calls; Genotyped: SNV density in the complete variant callset (based on VQSR PASS variants only).

Table S3. Percentage of bases in GRCh38 that could not be lifted over from GRCh37 within the GIAB confident regions.

Chromosome	Total Bases	Excluded Bases	% excluded
chr1	204,611,061	184,510	0.09
chr2	205,802,574	61,406	0.03
chr3	185,150,433	379,472	0.205
chr4	145,819,089	9,406	0.006
chr5	149,960,070	29,458	0.02
chr6	158,880,737	850,506	0.535
chr7	134,795,953	189,398	0.141
chr8	124,861,370	10,020	0.008
chr9	102,169,018	161,781	0.158
chr10	118,682,140	732,144	0.617
chr11	120,709,213	66,604	0.055
chr12	115,312,577	82,281	0.071
chr13	88,943,259	26,685	0.03
chr14	83,001,506	10,628	0.013
chr15	70,606,427	872	0.001
chr16	40,540,261	11,918	0.029
chr17	65,696,526	363,845	0.554
chr18	57,136,354	19,660	0.034
chr19	45,282,466	32,111	0.071
chr20	55,289,390	164,975	0.298
chr21	30,212,100	2,906	0.01
chr22	26,322,210	907	0.003
chrX	109,267,367	72,685	0.067

Table S4. Summary of the high coverage panel phasing accuracy evaluation stratified by chromosome.

Chromosome	No. of assessed HET pairs	No. of switch errors	SER
chr1	175,781	142	8.08E-04
chr2	191,683	138	7.20E-04
chr3	163,952	82	5.00E-04
chr4	168,622	60	3.56E-04
chr5	152,531	72	4.72E-04
chr6	163,088	60	3.68E-04
chr7	135,374	82	6.06E-04
chr8	126,465	76	6.01E-04
chr9	102,953	275	2.67E-03
chr10	123,322	64	5.19E-04
chr11	115,324	58	5.03E-04
chr12	109,988	62	5.64E-04
chr13	86,161	35	4.06E-04
chr14	75,916	97	1.28E-03
chr15	65,423	56	8.56E-04
chr16	73,588	72	9.78E-04
chr17	60,883	90	1.48E-03
chr18	68,376	36	5.27E-04
chr19	56,773	62	1.09E-03
chr20	54,650	42	7.69E-04
chr21	33,560	41	1.22E-03
chr22	34,542	52	1.51E-03
chrX	73,794	362	4.91E-03

The high coverage panel was phased using statistical phasing with pedigree-based correction (using SHAPEIT2-duohmm), except for chromosome X, which was phased using statistical phasing as implemented in the Eagle2 software (see Methods for more details). Switch error rate (SER) was computed relative to the Platinum Genome, NA12878, gold standard truth set.

Table S5. Count of SV sites across 3,202 samples and SVs per sample.

	# SV Sites across 3,202 samples			#SVs / sample		
SV TYPE	GATK-SV	SVTools	Absinthe	GATK-SV	SVTools	Absinthe
INS	48,333	75,283	7183	3,019	1,761	2,270
DEL	89,445	65,184	-	3,783	3,417	-
DUP	26,353	10,594	-	990	459	-
INV	381	1,447	-	12	127	-
BND	82,218	26,152	-	-	2,188	-
CPX	3,624	-	-	216	-	-
CTX	16	-	-	1	-	-
MCNV	674	-	-	385	-	-
ALL	251,044	178,660	7,183	8,406	7,952	2,270

Table S6. Quality of SVs evaluated by PacBio support and inheritance.

		All SVs		Callset specific		Shared with other callset	
	SV TYPE	gatksv	Absinthe/ SVTools	gatksv	Absinthe/ SVTools	gatksv	Absinthe/ SVTools
Proportion of VaPoR Supported SVs	INS	92.90%	97.60%	89.80%	96.30%	98.40%	99.00%
	DEL	88.00%	92.80%	71.40%	76.20%	92.60%	95.30%
	DUP	89.60%	88.10%	87.20%	62.70%	94.90%	95.40%
	INV	97.10%	47.60%	75.00%	44.80%	100%	55.70%
Overlap with PacBio Callsets	INS	93.20%	97.70%	90.00%	96.60%	99.20%	99.00%
	DEL	90.50%	94.10%	72.10%	79.40%	96.90%	97.10%
	DUP	3.30%	4.50%	3.90%	8.10%	1.70%	2.50%
	INV	20.30%	18.10%	18.50%	13.70%	30.40%	32.50%
de novo Rate	INS	2.90%	1.90%	4.00%	1.70%	0.90%	2.10%
	DEL	4.70%	1.30%	10.60%	5.30%	2.60%	0.50%
	DUP	11.90%	0.50%	13.80%	1.30%	6.90%	0.00%
	INV	2.80%	11.30%	2.90%	13.70%	2.00%	3.60%